A MICROMECHANICS-BASED CLASSIFICATION OF THE REGIMES DELINEATING THE BEHAVIOUR OF GAP-GRADED SOILS

Peter Adesina, Antoine Wautier, Nadia Benahmed

A MICROMECHANICS-BASED CLASSIFICATION OF THE REGIMES DELINEATING THE BEHAVIOUR OF GAP-GRADED SOILS

Peter Adesina[1]*, Antoine Wautier[2], Nadia Benahmed[3]

[1,2,3]INRAE, Aix-Marseille University; UMR RECOVER, 3275 Rte Cézanne, CS 40061, 13182 Aix-en-Provence, France

*Corresponding author. E-mail addresses: peter.adesina@inrae.fr, greatpetson121@gmail.com (P. Adesina); antoine.wautier@inrae.fr (Antoine Wautier); nadia.benahmed@inrae.fr (Nadia Benahmed)

Abstract

This study presents a micromechanical evaluation of the regimes delineating the behaviour of gap-graded granular assemblies, using discrete element simulations. Dense and loose bimodal assemblies of different fines content were prepared and subjected to drained triaxial compression until the critical state was reached. The regimes delineating the behaviour of the assemblies were evaluated, characterised and their significance discussed. While two regimes demarcated by the threshold fines content were identified based on the analysis of the macroscale characteristics of the assemblies, up to four regimes were identified based on the contributions of the particle size fractions and contact types to the total mean stress. Contrary to previous studies according to which fines control the mechanical behaviour of gap-graded assemblies from the threshold fines content, f_c^{th}, we found that the fines do not play a primary role in stress transmission until beyond a significantly larger fines content, f_c^{eq} (the equivalent fines content), which depends on density and stress state. Based on the correlation found between the critical state strength and the stress-based skeleton void ratio proposed in this study, we conclude that stress-based skeleton void ratio can be useful in understanding the mechanical response of gap-graded materials at the critical state.

Keywords: Gap-graded assemblies, regimes, density, triaxial compression, DEM

[1]Post doctoral researcher, INRAE, Aix-Marseille University; UMR RECOVER, 3275 Rte Cézanne, CS 40061, 13182 Aix-en-Provence, France. Email: peter.adesina@inrae.fr; greatpetson121@gmail.com

[2]Research Fellow, INRAE, Aix-Marseille University; UMR RECOVER, 3275 Rte Cézanne, CS 40061, 13182 Aix-en-Provence, France. Email: antoine.wautier@inrae.fr

[3]Research Fellow, INRAE, Aix-Marseille University; UMR RECOVER, 3275 Rte Cézanne, CS 40061, 13182 Aix-en-Provence, France. Email: nadia.benahmed@inrae.fr

1. Introduction

Soil mixtures containing a coarser and a finer fraction (as in silty sands, sandy gravels, etc.) are abundant in nature. It is well established that the mechanical behaviour of these mixtures depends on the proportions of the coarser and the finer fraction within the mixtures. However, there is no consensus in the literature on specific fine contents delineating different behaviour for gap-graded granular mixtures. For example, as a result of the conceptual analysis presented in experimental studies, it has been suggested that the fines play a primary role in the shear behaviour of gap-graded assemblies beyond a threshold fines content (Thevanayagam et al., 2002); and control the behaviour beyond a limiting fines content (Lade & Yamamuro, 1997; Salgado et al., 2000; Skempton & Brogan, 1994; Vallejo, 2001). The threshold fines content is usually related to geometric properties, and in particular the measure of the minimum void ratio (Cubrinovski & Ishihara, 2002; Yang et al., 2005; Zuo & Baudet, 2015). From the threshold fines content, the fines start to disperse the coarse particles. The limiting fines content corresponds to the situation where the fines completely disperse the coarse particles (floating grains in a fine matrix) (Skempton & Brogan, 1994; Thevanayagam et al., 2002). Since quantifying the stress or the dispersion of individual particles within a matrix is difficult in experiments, it is almost impossible to ascertain the delineating fines content of the conceptual models without the use of a micromechanical framework.

In this regard, the discrete element method (DEM) proposed by (Cundall & Strack, 1979) has been found an effective numerical tool for probing the micromechanics of granular materials. DEM offers the opportunity to evaluate the assertions from the conceptual models in earlier experimental studies where the stress transmitted by individual particles cannot be determined. In the earlier studies where DEM has been used to assess the behaviour of gap-graded assemblies, the approach adopted involved determining the proportion of the stress transmitted by each particle size fraction and contact types. However, no consensus has been reached on the specific fines content delineating different behaviour; in fact, the existence of some of the specific fines contents suggested by experimental studies is sometimes questioned (as in Sufian et al., (2021)) or not identified.

In this study, we conducted four analyses organised into four sections to evaluate the regimes[4] delineating the behaviour of gap-graded sand-silt mixtures. In Section 3, we determined the macroscale and micromechanical behaviour of the assemblies of sand-silt mixtures with fines

[4] The word "regime" in this paper refers to zones of unique behaviour within the range of fines content in gap-graded assemblies.

content, f_c, within 10%≤ f_c≤70%; and assessed the existence of regimes delineating the characteristics of the assemblies. The macroscale characteristics considered are the void ratio, strength and dilatancy, while the micromechanical characteristic considered is the coordination number. We then conducted in Section 4, a particle-scale analysis of the contribution of the finer and the coarser fractions to the total mean stress transmitted by an assembly. This enabled a particle stress-based evaluation of the regimes delineating the behaviour of the assemblies. Following this, in Section 5, we conducted a contact-scale analysis of the contribution of each contact type to the total mean stress, again to identify existing regimes. Finally, in Section 6, we present a stress-based skeleton void ratio as an alternative void ratio index to interpret the strength properties of the granular mixtures studied. We assessed the performance of alternative void ratio indexes such as the mechanical and the void ratio (global), in interpreting the strength exhibited by the granular mixtures studied, at both the peak and the critical state. An assessment of the internal instability of the gap-graded assemblies (i.e. their susceptibility to internal erosion) is beyond the scope of this study. However, the implications of the findings with respect to internal erosion are discussed in the conclusion.

2. Numerical Simulation approach

The DEM simulations in this study were conducted using the open-source code YADE (Šmilauer et al, 2021). All assemblies were generated to have a bimodal grading of fine particles with diameter, D_f=0.375 mm and coarse particles with diameter D_c=3.075 mm such that the size ratio, $\lambda = D_c/D_f$ = 8.2. The bimodal grading is considered the simplest type of gap-graded material and was employed in this study to ensure the results obtained are solely from the interaction between the coarser and the finer fractions without the interference of the grading effect from within either of the fractions. The size ratio value was selected sufficiently large to allow for fine migration in the pore space (should water flow be considered) (Lade et al., 1998; Rahman et al., 2008; Shire et al., 2016; Thevanayagam et al., 2002).

After a parametric study to determine the representative element volume (REV), each assembly contains 100,000 particles (Fig.1). Increasing the sample size to 200,000 particles for the f_c = 30% case at both the dense and loose states did not significantly influence the stress-strain responses (see Appendix A). The slight sensitivity to sample size observed in the volumetric strains was also reported in the DEM study on REV for granular materials by Adesina et al., (2022) and can be attributed to the small variation in the initial void ratio of the assemblies.

Table 2 shows the number of the fines and the coarse particles for each percentage of fines content, f_c (%).

The assemblies studied here were prepared by subjecting them to isotropic compression at 100 kPa within six frictionless walls. The standard linear elasto-plastic model was employed to simulate the interactions between particles. Table 1 shows the simulation parameters employed in the simulations. Following Jiang et al., (2018), the material density in the simulations was scaled to 1000 times the original value in order to increase the critical time step, $\Delta t_{cr} \propto r\sqrt{\rho/E}$, where r is the particle radius, ρ is the density and E is the Young's modulus. A fraction ($0.9\Delta t_{cr}$) of this critical time step was then applied to ensure numerical stability. While this density scaling approach was adopted for computational efficiency, it does not compromise the quasi-static conditions of the simulations as long as the inertial number remains sufficiently small (Thornton, 2000; Thornton & Anthony, 1998). Based on the standard practice adopted in prior DEM studies including (Thornton, 2000) for assembly preparation, here, assemblies of different initial densities were generated by using a friction coefficient μ=0.03 for the dense assemblies and μ=0.5 for the loose assemblies, during isotropic compression. The void ratio of the dense assemblies is denoted e_{min}, while the void ratio of the loose assemblies is denoted as e_{max}. It is important to note that these e_{min} and e_{max} values cannot be directly mapped to the values obtained using standard procedures employed in experiments.

After isotropic compression, the assemblies were subjected to triaxial compression under a constant confining pressure of σ_{xx}=σ_{yy}=100 kPa[5] in both the x-direction and y-direction and a strain rate of 0.01 s^{-1} in the z-direction. A numerical damping coefficient of 0.05 is used. These conditions ensured that for our simulations, the inertial number for the coarse particles, I_{dmax} = 1.60 x 10^{-4}, and that for the fines, I_{dmin} = 1.95 x 10^{-5}, therefore the simulations were deemed quasi-static (da Cruz et al., 2005). Prior to shearing, additional number of cycles at μ=0.5 was applied to equilibrate the assemblies. Also, the unbalanced force ratio[6] was checked to remain below a limit of 0.01 to guarantee static equilibrium. All assemblies were sheared at μ=0.5 regardless of the friction coefficient used during the assembly preparation stage. A total of 22 shearing simulations were conducted in this study (11 fines contents are considered for 2 relative densities) (Table 2).

[5] Throughout this paper, soil mechanics conventions are used with compression being positive and extension being negative.

[6] The maximum resultant force on the different grains divided by the mean contact force.

Table 1 Simulation parameters

Parameter	Value
Diameter of coarse particles, D_c, mm	3.075
Diameter of fine particles, D_f, mm	0.375
Particle size ratio D_c / D_f	8.2
Particle density, ρ, kg/m^3	2700×10^3
Contact law	Elasto-frictional
Inter-particle friction coefficient during isotropic compression	0.03 (dense), 0.5 (loose)
Inter-particle friction coefficient during shearing	0.5
Wall-particle friction coefficient	0
Particle normal stiffness, k_n, N/m^2	3.56 x 10^8
Stiffness ratio	1.0

Table 2 Number of particles for each assembly

Specimens		Percentage of fine particles by weight										
		10%	15%	20%	25%	30%	35%	40%	45%	50%	60%	70%
Number of particles	Coarse	1,612	1,021	723	543	423	337	272	222	182	121	78
	Fine	98,388	98,979	99,277	99,457	99,577	99,663	99,728	99,778	99,818	99,879	99,922
	Total	100,000										

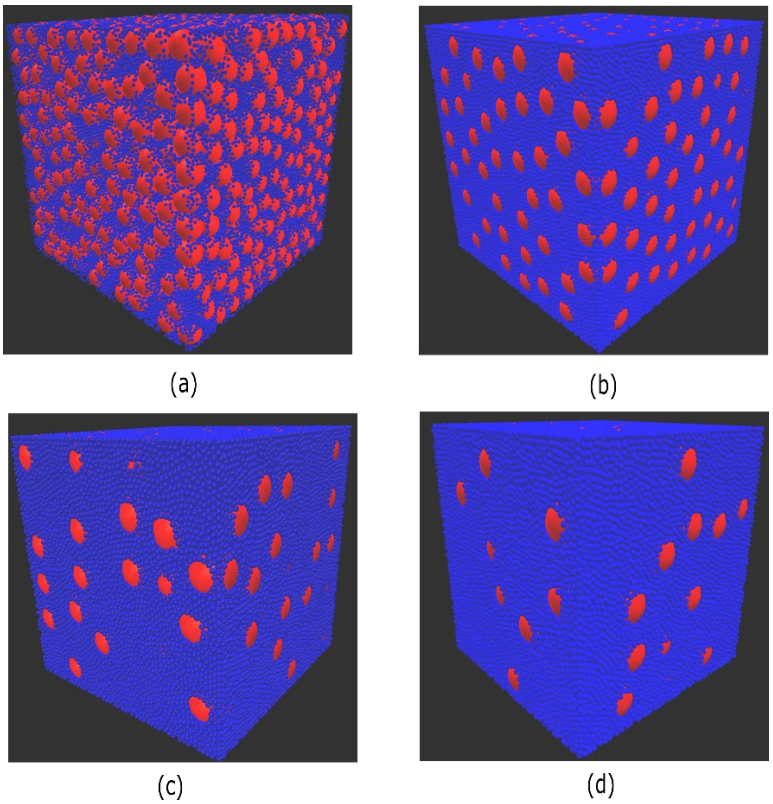

Fig. 1. Dense specimens with different percentages of fines content: (a) f_c = 10 % (b) f_c = 30 % (c) f_c = 50 % (d) f_c = 70 %

3. Macro-scale and micromechanical characteristics of the binary mixtures for varying fines content.

The initial void ratios of the gap-graded assemblies with different fines content are plotted in Fig. 2a. As earlier mentioned, the void ratio of the dense and loose assemblies studied are denoted as e_{min} and e_{max}, respectively. In both the dense and the loose assemblies, two regimes of distinct trends are observed. The first regime is characterised by a reduction in the void ratio as f_c increases. This is as a result of the fines progressively filling the voids within the coarse particles. At a certain fines content referred to as the critical fines content (Skempton & Brogan, 1994), the threshold fines content, f_c^{th} (Lade et al., 1998; Thevanayagam et al., 2002), or the transitional fines content (Yang et al., 2005), the voids within the coarse particles are fully filled by the fines. The second regime corresponds to f_c>f_c^{th} and it is characterised by an increase in the void ratio as the f_c increases. In this regime, the fines progressively disperse the coarse particles, thereby causing an increase in the void ratio. These two regimes have been reported in previous studies involving gap graded materials (Cubrinovski & Ishihara, 2002; Kuerbis, 1989; Lade & Yamamuro, 1997; W. Li et al., 2023; Y. Li et al., 2022; Minh et al., 2014; Sufian et al., 2021; Vallejo, 2001; Zuo & Baudet, 2015). The two identified regimes are referred to as the underfilled and the overfilled categories by dam engineers (ICOLD, 2013; Shire et al., 2014), and are demarcated by the threshold fines content (i.e. the filled state).

One particular feature that is less frequently highlighted in the literature is the fact that the f_c^{th} slightly depends on the relative density of the mixture. The f_c^{th} here was attained at $f_c = 0.30$ for the dense assemblies whereas f_c^{th} = 0.35 for the loose assemblies. Indeed, in looser assemblies, the pores are larger and more fine grains are required to fill the voids before the coarse grains are dispersed. This is in agreement with the 3D DEM study of binary mixtures by Minh et al., (2014). In the literature, different limits within which the threshold fines content is attainable have been reported. For example, Skempton & Brogan (1994) suggested that in practice, f_c^{th} is unlikely to occur beyond 24% and 29% for dense and loose packings of sandy-gravels, respectively. Lade & Yamamuro (1997) suggested a limit of 20%-30% fines content for sand-silt mixtures of different gradations. Other studies show that the f_c^{th} can occur outside Skempton and Brogan's and Lade & Yamamuro's limits, depending on the grain size distribution and the particle shape considered (Evans & Zhou, 1995; Sarkar et al., 2020; Shire et al., 2014; Sufian et al., 2021; Wang et al., 2022; Zuo & Baudet, 2015).

The conceptual distinction between underfilled and overfilled assemblies led Yin et al., (2014) to propose the following equation for determining the void ratio, e, for sand-silt mixtures at different fines content f_c:

$$e = [e_{hc}(1-f_c) + af_c]\frac{1-tanh[\xi(f_c-f_{th})]}{2} + e_{hf}\left(f_c + \frac{1-f_c}{(R_d)^m}\right)\frac{1+tanh[\xi(f_c-f_{th})]}{2} \quad (1)$$

where e_{hc} is the void ratio of the pure sand, e_{hf} is the void ratio of the pure silt , a is a material constant depending on the fabric structure of the soil mixture, ξ is a material constant controlling the transition from a coarse grain matrix to a fine grain matrix, f_{th} is the threshold fines content at which the coarse and fine grains contribute equally to the global void ratio, R_d is the ratio of the mean size of the coarse grains, D_{50}, to the mean size of the fine grains d_{50} and m ($0 < m < 1$) is a coefficient that depends on grain characteristics and fine grain packing. The fitting parameters for the dense assemblies are e_{hc}= 0.67;a = -0.64; ξ = 16.6; f_{th} = 0.28; e_{hf}=0.62; m=0.73 while the parameters for the loose assemblies are e_{hc}= 0.71;a = 0.03; ξ = 12.6; f_{th} = 0.26; e_{hf}=0.76; m=0.99. It is clear, as shown in Fig. 2a, that this phenomenological equation fits our data.

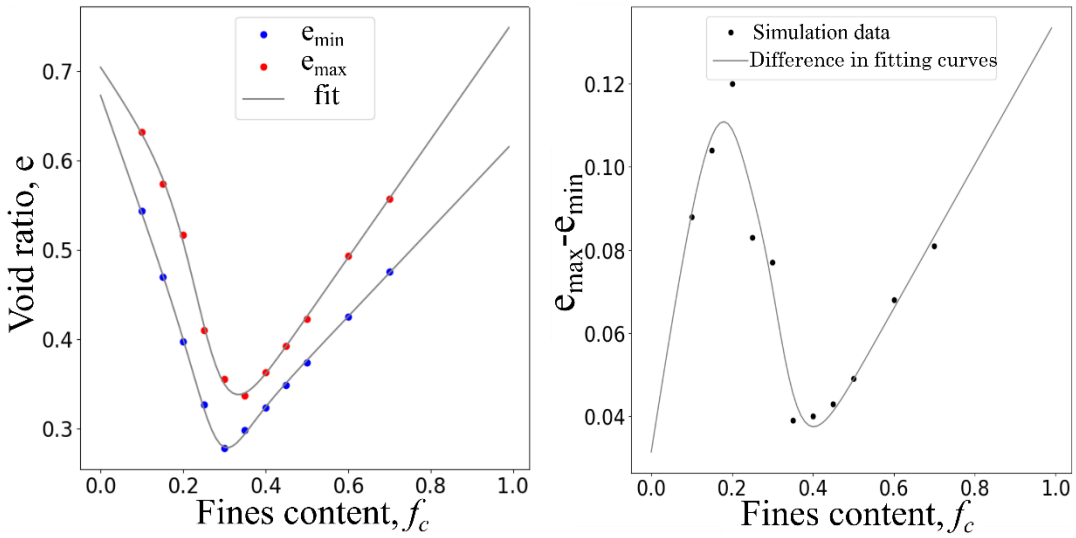

Fig. 2. Effect of fines content, f_c, on (a) the initial void ratio, e, (b) the range of attainable void ratios, $e_{max} - e_{min}$ for the assemblies of binary mixture studied

Fig. 2b shows the range of attainable void ratio, $e_{max} - e_{min}$, for each fines content. $e_{max} - e_{min}$ for the underfilled assemblies (i.e. f_c<f_c^{th} = 35%) is generally higher in comparison to the overfilled assemblies. In the underfilled assemblies, we observed an initial increase in $e_{max} - e_{min}$ with the fine content which indicates that the fines do not simply fill the voids in the loose case. Indeed, they enable the formation of larger pore structures.

Fig. 3 shows the evolution of the stress ratio, q/p, and the volumetric strain (ϵ_{vol}), against the axial strain (ϵ_a), for the dense assemblies of binary mixtures with different fines content. The corresponding data for the loose assemblies are presented in Fig. 4. The assemblies were sheared until $\epsilon_a \approx 0.5$ in order to reach the critical state. Here, the deviatoric stress, $q = \sigma_{zz} - (\sigma_{yy} + \sigma_{xx})/2$ and the mean stress, $p = (\sigma_{zz} + \sigma_{yy} + \sigma_{xx})/3$ (axisymmetric conditions). In a typical fashion to sand behaviour, the q/p for the initially dense assemblies increased until reaching a peak and thereafter softened to the critical state where the q/p fluctuates around a mean value, with more pronounced fluctuations observed for $f_c < 45\%$ (Fig. 3a &b). The stiffness of the packings as influenced by the fines content is shown in the inset of Fig. 3a-c. These dense assemblies exhibited a dilative volumetric response ($\epsilon_{vol} < 0$) during shearing (Fig. 3d-f). At large strains ($\epsilon_a > 35\%$), ϵ_{vol} tend to increase from f_c = 10% to f_c = 35% (indicating a less dilative behaviour), and then decreased with further increase in the f_c. In contrast, at small strains ($\epsilon_a < 2\%$) (inset of Fig. 3d-f), a more dilative response was observed from f_c = 10% to f_c^{th}=30% as ϵ_{vol} decreases. The stress ratio q/p for the initially loose assemblies (Fig. 4a-c) increased monotonically from the beginning of shearing to the critical state without significant softening observed, as expected. These loose assemblies exhibited a contractive response ($\epsilon_{vol} > 0$) during shearing (Fig. 4d-f).

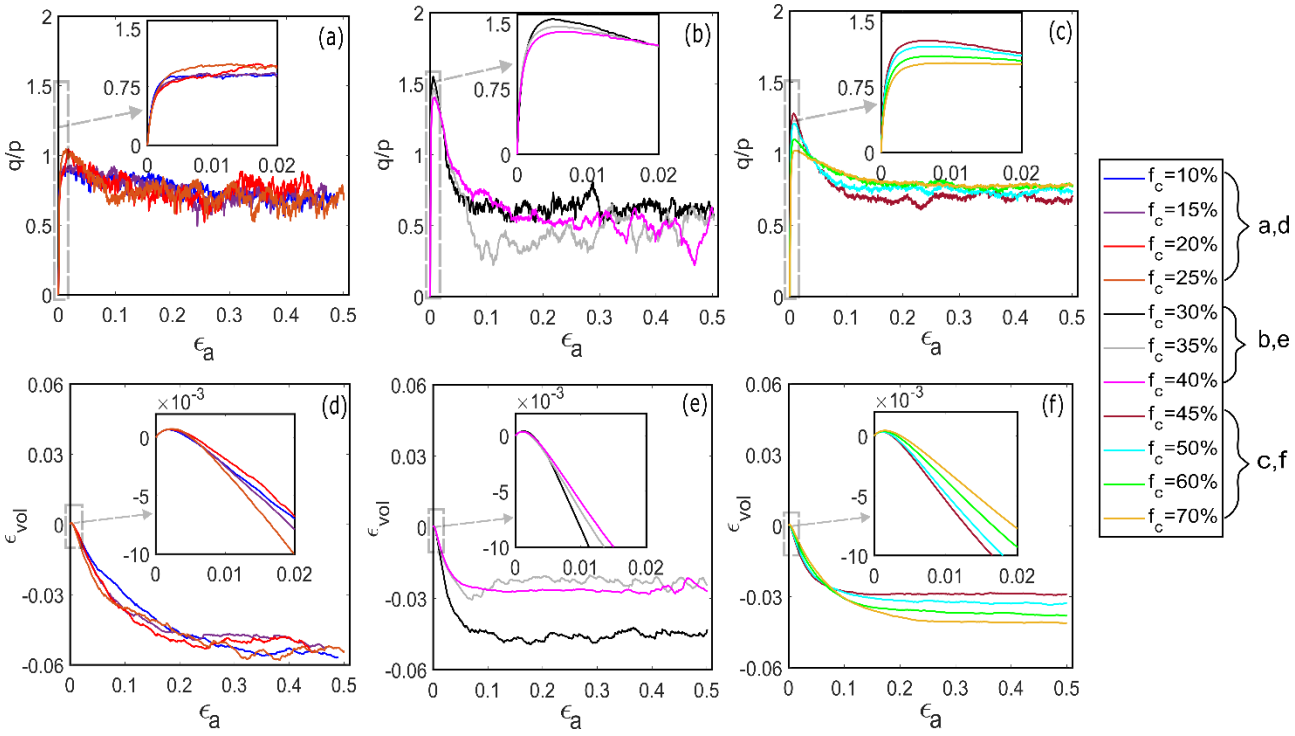

Fig. 3. Effect of fines content, f_c, on the stress-strain and the volumetric strain responses for dense assemblies (a,d) f_c = 10%-25% (b,e) f_c = 30%-40% (c,f) f_c = 45%-70%. Inset graphs correspond to the start of the loading.

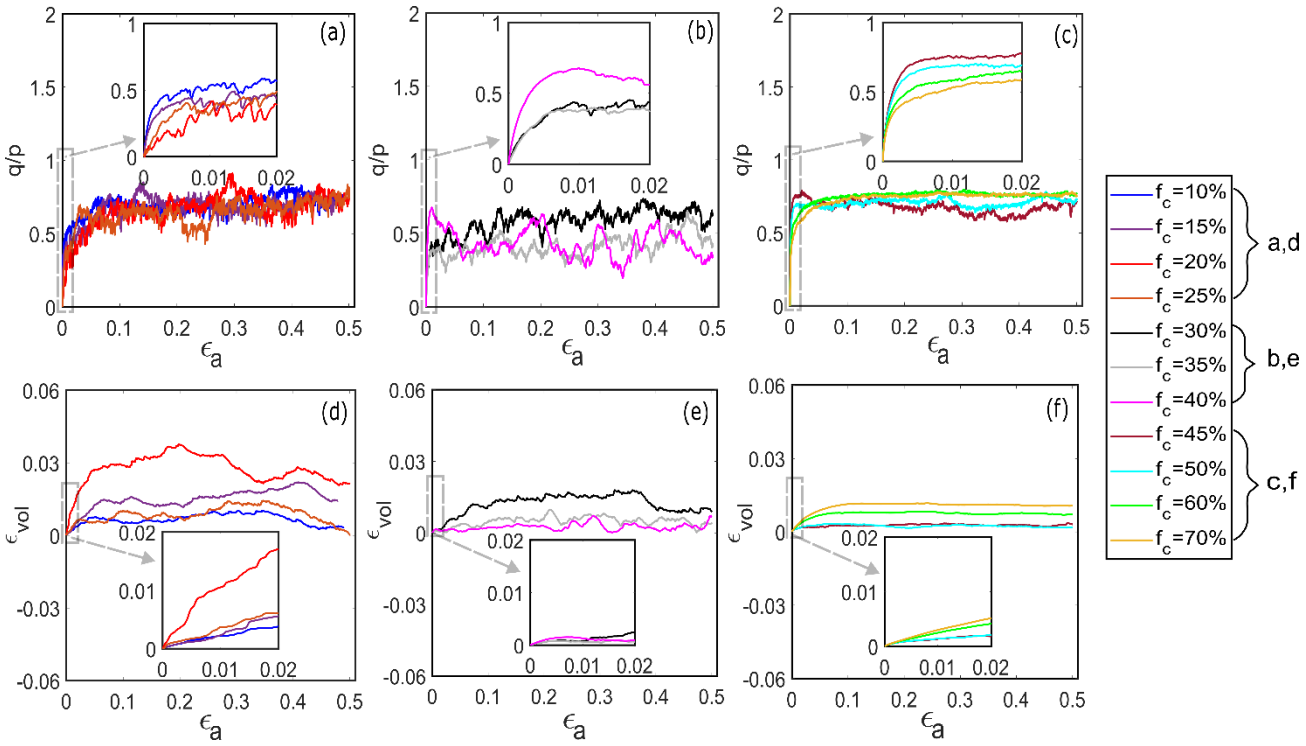

Fig. 4. Effect of fines content, f_c, on the stress-strain and the volumetric strain responses for loose assemblies (a,d) f_c = 10%-25% (b,e) f_c = 30%-40% (c,f) f_c = 45%-70%. Inset graphs correspond to the start of the loading.

In Fig. 5a, the stress ratio q/p at the peak, $(q/p)_{peak}$, is plotted against f_c alongside the void ratio at the peak, e_{peak}, for comparison. Similarly, Fig. 5b shows the plot of the critical state stress ratio, $(q/p)_{crit}$, against f_c alongside the critical state void ratio, e_{crit}. Here, the $(q/p)_{peak}$ is the maximum q/p attained between the start of shearing and the critical state; $(q/p)_{crit}$ and e_{crit} are mean values determined from the start of the critical state to the end of shearing. The critical state marks the state at which there is no noticeable change in the void ratio or the volume of a sample during shearing. This generally occurred at $\epsilon_a > 0.35$ for the studied assemblies. As the fines progressively fill the voids within the coarse particles in the underfilled regime where $f_c < f_c^{th}$, the assemblies become denser such that $(q/p)_{peak}$ increases with f_c until the threshold fines content where the highest $(q/p)_{peak}$ is attained (Fig. 5a). For $f_c > f_c^{th}$, the fines disperse the coarse particles leaving more voids within the assemblies thereby causing a monotonic decrease in $(q/p)_{peak}$ as f_c increased.

In agreement with earlier experimental studies on Ottawa sand and Carmague silty sand with $f_c \leq 20\%$ under drained shearing (Benahmed et al., 2015; Chang & Yin, 2011; Salgado et al., 2000), a marginal increase in $(q/p)_{crit}$ was observed from f_c = 10% to f_c = 20%. This is followed by a significant decrease in $(q/p)_{crit}$ until f_c = 40%, and finally a monotonic increase

until f_c = 70% (Fig. 5b). The e_{crit} follows a similar trend as the e_{peak}, although the threshold fines content shifted from f_c^{th}=30% at the initial state (Fig. 5a) to f_c^{th}=35% at the critical state (Fig. 5b). While e_{peak} could be used to explain the trend observed for $(q/p)_{peak}$, $(q/p)_{crit}$ does not correlate with e_{crit}. In Section 6, we provide a discussion on the use of an alternative void index, the stress-based skeleton void ratio, to explain the trend observed at the critical state. It is worthy of note that having a lot of fine grains filling the void space increases the peak strength but decreases the critical state strength. This might be interpreted in the capacity of fine grains to i) provide lateral support to force chains if the initial state is dense, but at the same time ii) act as ball bearings at critical state and ease shearing with limited deviatoric stress.

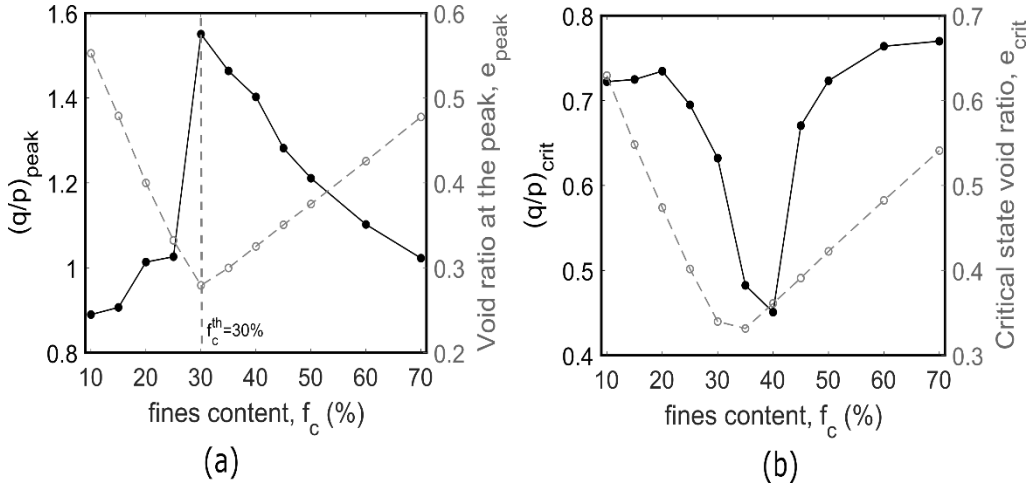

Fig. 5 Effect of fines content on (a) stress ratio at peak, $(q/p)_{peak}$, for the dense assemblies, and peak void ratio, e_{peak} (b) critical state stress ratio, $(q/p)_{crit}$, (unique value for dense and loose assemblies), and critical state void ratio, e_{crit}.

Fig. 6a shows the maximum dilatancy rate, $(-\mathrm{d}\varepsilon_v/\mathrm{d}\varepsilon_a)_{max}$ against f_c. In the underfilled regime, $(-\mathrm{d}\varepsilon_v/\mathrm{d}\varepsilon_a)_{max}$ for the dense assemblies increased from f_c = 10% until the threshold fines content f_c^{th}=30%, as the fines progressively fill the void space (Fig. 6a). For f_c>f_c^{th}, $(-\mathrm{d}\varepsilon_v/\mathrm{d}\varepsilon_a)_{max}$ decreased monotonically with an increase in f_c. The increase in dilatancy observed within the underfilled regime was also reported for Ottawa sand having $f_c \leq 20\%$, under drained triaxial shearing (Chang & Yin, 2011; Salgado et al., 2000); and was attributed to increased particle interlock as the fines occupy the voids within the coarse particles (Kuerbis, 1989; Salgado et al., 2000). Indeed, for the assemblies of binary mixture studied here, there is a correlation between the maximum dilatancy angle, ψ_{max} and the initial void ratio, e_{min}, (Fig. 6b), where $\psi_{max}= \sin^{-1}\left[\left((-\mathrm{d}\varepsilon_v/\mathrm{d}\varepsilon_a)_{max}\right)/\left(2+(-\mathrm{d}\varepsilon_v/\mathrm{d}\varepsilon_a)_{max}\right)\right]$ following (Xiao et al., 2017). A linear relationship was also established between the peak friction angle, ϕ_p and the

ψ_{max} (Fig. 6c), where the friction angle, $\phi = \sin^{-1}\left[\left(\sigma_{zz} - \sigma_{yy}\right)/\left(\sigma_{zz} + \sigma_{yy}\right)\right]$. This relationship has been found in earlier studies for clean sands (Adesina et al., 2024; Bolton, 1986; Vaid & Sasitharan, 1992), and was also reported for sand-silt mixtures having $f_c \leq 20\%$ in the experimental study on sand with non-plastic fines (Xiao et al., 2017).

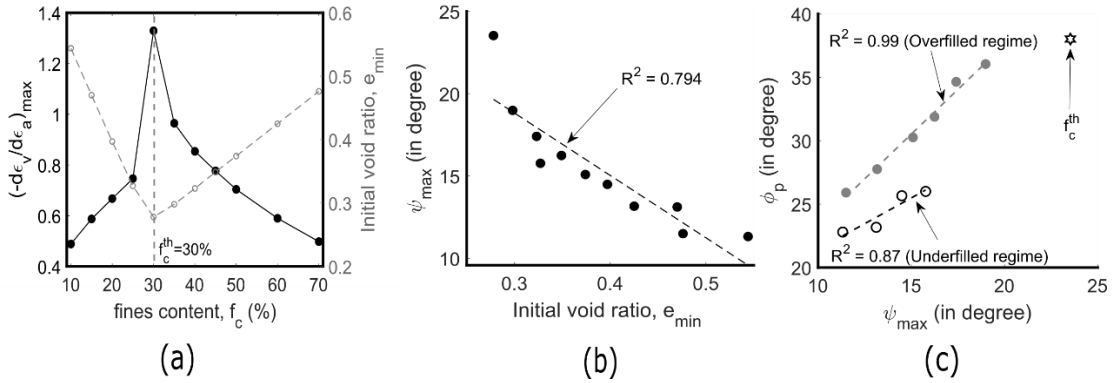

Fig. 6 (a) Effect of fines content, f_c, on the maximum dilatancy rate, $(-\mathrm{d}\varepsilon_v/\mathrm{d}\varepsilon_a)_{max}$. Relationship between (b) maximum dilatancy angle, ψ_{max} and initial void ratio, e_{min} (c) peak friction angle, ϕ_p, and maximum dilatancy angle, ψ_{max} for dense assemblies of binary mixture.

The coordination number, i.e. the average number of contacts per particle in a granular system is the simplest measure of the connectivity of the contact network which is related to the structural stability of the system (Thornton, 2015). Here, we employ the mechanical coordination number as a micromechanical parameter to identify and characterise the regimes delineating the behaviour of gap-graded materials. The mechanical coordination number, Z_m, is defined as the average number of contacts per particle when the particles which do not contribute to force transmission (i.e., particles with less than two contacts which are referred to as rattlers) are excluded[7]. Thornton (2000) defined the Z_m as:

$$Z_m = \frac{(2N_c - N_1)}{N_p - N_1 - N_0} \tag{2}$$

where N_c is the total number of contacts, N_p is total number of particles and N_0 and N_1 are the number of particles with zero and one contact in the granular system, respectively. Figs. 7a-c show Z_m for all particles, Z_{mc} for the coarse particles only, and Z_{mf} for the fine particles only, respectively, alongside the void ratio, e, at the initial, the peak and the critical states. While Z_m considers all particles, Z_{mc} and Z_{mf} considers only the contacts made by the coarse particles and the fine particles, respectively[8]. Figs. 7d-e show the number of fines and coarse particles

[7] Note that the coordination number of particles with more than two contacts accounts for the contacts from particles with only one contact in the standard definition of Z_m.
[8] The contacts made by the coarse particles include both the coarse-coarse and the coarse-fine contacts while the contacts made by the fine particles include both the fine-fine and the coarse-fine contacts.

that do not contribute to force transmission (i.e. the fines-rattlers and coarse-rattlers) at the initial, the peak and the critical states. Generally, two trends demarcated by the f_c^{th} can be observed in Fig. 7a; a decrease in the Z_m for f_c<f_c^{th} (although the decrease is less significant for the dense assemblies at the initial state); and a monotonic increase for f_c>f_c^{th}. The trends observed here are similar to the data shown in the DEM study by Liu et al., (2022) for the Z_m of sand-silt mixtures having particle size ratio, λ = 8.4 and 18.1, and at the initial states. Generally, an initial increase in the f_c resulted in no change in the Z_{mc} and the Z_{mf} until f_c^{th}, after which a monotonic increase followed (Figs. 7b & c). The monotonic decrease in the number of fines-rattlers from f_c^{th} (Fig. 7d) indicates an increase in the number of fines mobilised in force transmission as f_c increases. As expected, the number of coarse-rattlers decreased with an increase in f_c until f_c^{th}, beyond which no rattler exists among the coarse particles (Fig. 7e).

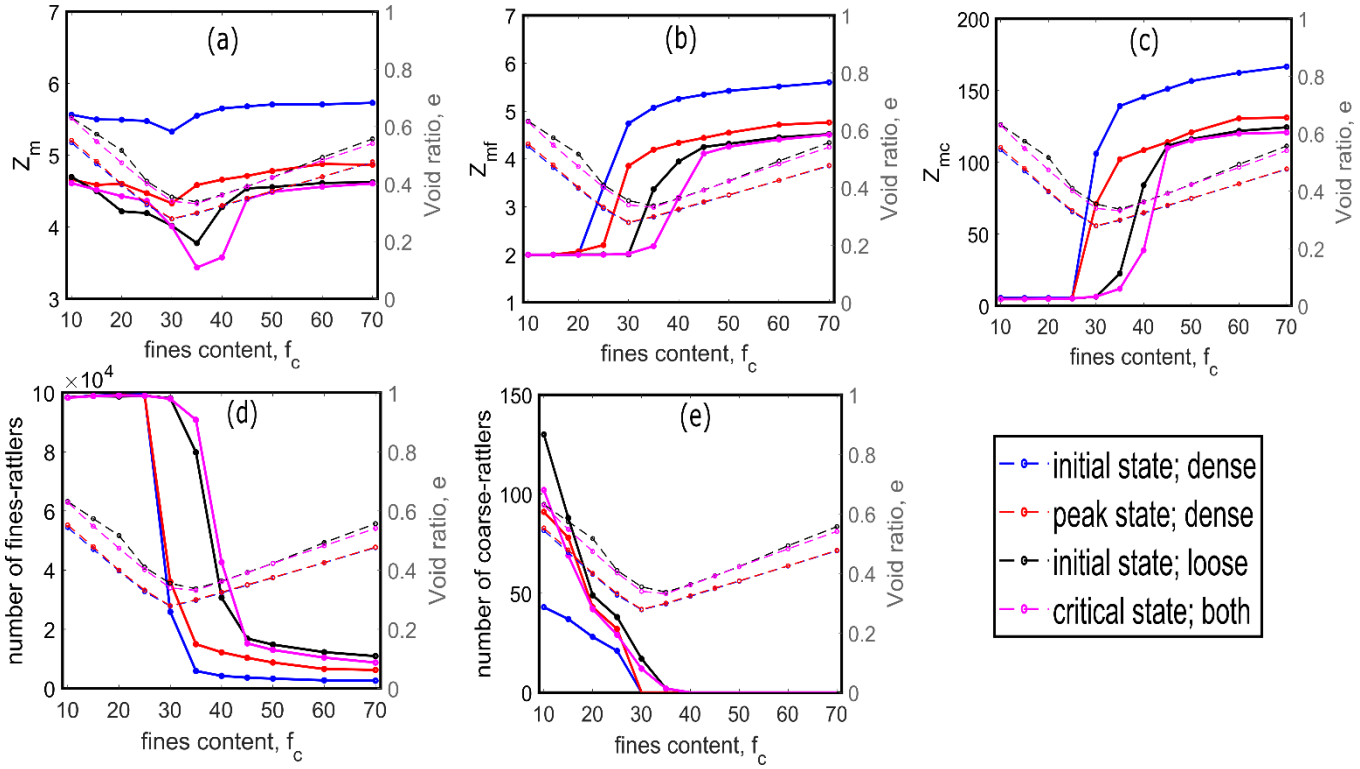

Fig. 7 Effect of fines content on the (a) mechanical coordination number, Z_m, for all particles (b) Z_{mc} for coarse particles (c) Z_{mf} for fine particles (d) number of fines-rattlers (e) number of coarse-rattlers within assemblies of binary mixture.

Fig. 8a shows the contact lost or gained during shearing, ΔZ, determined here as $Z_{ini} - Z_{crit}$, where Z_{ini} and Z_{crit} are the coordination number at the initial states and at the critical state, respectively. Fig. 8b shows the excess friction angle, which indicates the strain softening exhibited by the assemblies. From these figures, we observe the emergence of three groups of

f_c values with similar ΔZ and ϕ_p-ϕ_c values. This suggests the existence of three regimes, the first being $f_c < f_c^{th}$ where $\Delta Z \approx 0$ and strain softening is relatively minimal. In the second regime delineated by $f_c^{th} \leq f_c < 45\%$, ΔZ is highest, suggesting that the highest amount of contacts were lost within this regime during shearing. This is accompanied by significant softening occurring within the regime, in agreement with the DEM study by Adesina et al., (2024), where a linear relationship is established between the degree of softening and the contact loss during shearing by linearly-graded granular assemblies. The significant loss of contacts exhibited by the assemblies in this regime can be linked to the large fluctuations in their shearing responses at the critical state (see Figs. 3 & 4). It has been shown in the DEM study by Adesina et al., (2022) that the magnitude of fluctuations in the shearing responses of granular assemblies at the critical state increases with a decrease in the total number of contacts in the assemblies. This observation can also be related to the size of the REV, which depends on the fine contents. While the condition is largely met for small and large fine contents with 100,000 grains, this is less the case for intermediate fine contents in which local microstructure rearrangements reflect more in the macroscopic response. This is observed in Fig. 16 through the evolution of the boundary term in the stress decomposition. In Appendix A, we showed that our sample size of 100,000 particles can be considered as a REV.

In the third regime (i.e. $f_c \geq 45\%$), relatively minimal ΔZ is observed; the strain softening within this regime transitions from moderate to minimal. ΔZ values in the last two regimes are higher for dense assemblies in comparison to the loose assemblies, for the same f_c value; $\Delta Z<0$ for the loose assemblies in regime 3 indicating an ultimate contact gain. While Skempton & Brogan (1994) and Thevanayagam et al., (2002) provided a conceptual delineation of the regimes based on void ratio, here, we provide a mechanistic delineation of the regimes with our analysis of contact evolution and strain softening. In Table 3, we present a summary of the unique trends observed for each of the three regimes identified based on our analysis of the macromechanical and the micromechanical characteristics of the studied gap-graded assemblies.

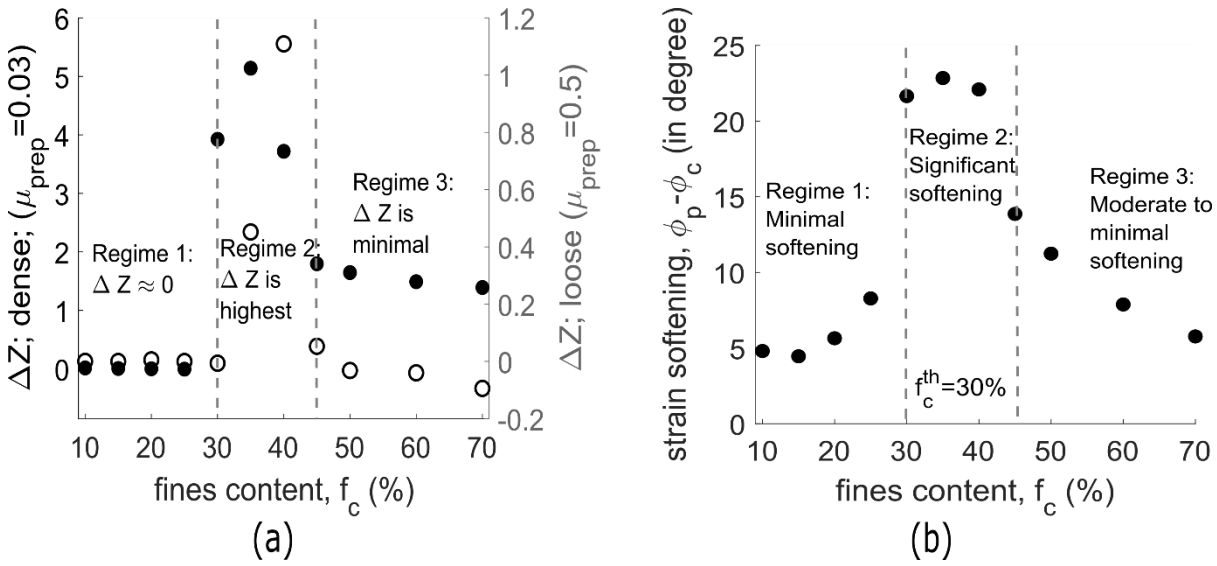

Fig. 8 (a) Change in coordination number during shearing, ΔZ (filled circle for dense assemblies and open circles for loose assemblies). $\Delta Z>0$ means contact lost and $\Delta Z<0$ means contact gained during shearing. (b) excess friction angle (strain softening), ϕ_p-ϕ_c for dense assemblies of binary mixture.

Table 3: Summary of regime based on macromechanical and micromechanical characteristics

Δ in parameters as the f_c ↑	Regime 1 ($f_c < f_c^{th}$)	Regime 2 ($f_c^{th} < f_c$<45%)	Regime 3 (f_c>45%)
e_{ini}; e_{crit}	Decreases	Increases	
$(q/p)_{max}$	Increases	Decreases	
$(-d\varepsilon_v/d\varepsilon_a)_{max}$	Increases	Decreases	
Z_m	Decreases	Increases	Increases marginally to a plateau
Z_{mc}; Z_{mf}	No change	Increases	Increases marginally to a plateau
ΔZ	No change	Increases	Decreases marginally to a plateau
ϕ_p-ϕ_c	Increases	Plateau	Decreases

Note: When the data in Fig. 8 are considered, the boundary between Regime 2 and Regime 3 range between $f_c \in$ [35% ; 45%] depending on density. This range will also depend on the particle size distribution considered.

4. Particle based stress-transmission

Using the Love-Weber particle stress tensor as described in Nicot et al., (2013), the mean stress per particle, σ_{ij}^p, is calculated as:

$$\sigma_{ij}^p = \frac{1}{V^p} R_p \sum_{c=1}^{N_c^p} f_j^c \, \boldsymbol{n}_i \qquad (3)$$

where the summation runs over all contacts c made by the particle p. V^p is the particle volume, R_p is the radius of the particle, N_c^p is the number of contacts involving the particle, f_j^c is the contact force vector and $\boldsymbol{n}_i$ is the unit branch vector between two particles in contact. The stress tensor at the material point scale (i.e. for a large number of particles), σ_{ij}, is given as a weighted average of the particle stresses (by particle volume):

$$\sigma_{ij} = \frac{1}{V}\sum_{p=1}^{N_p} V^p \sigma_{ij}^p \qquad (4)$$

where V is the volume of the entire system and N_p is the number of particles in the system. σ_{ij} can be decomposed to the contribution of each particle category, i.e. fine and coarse, as:

$$\sigma_{ij} = \underbrace{\frac{1}{V}\sum_{p=1}^{N_p^c} V^p \sigma_{ij}^p}_{\sigma_{ij}^c} + \underbrace{\frac{1}{V}\sum_{p=1}^{N_p^f} V^p \sigma_{ij}^p}_{\sigma_{ij}^f} \qquad (5)$$

where N_p^c and N_p^f are the number of coarse and fine particles in the system, respectively[9]. The mean effective stress, p, for the entire system is calculated as:

$$p = \frac{\sigma_{xx} + \sigma_{yy} + \sigma_{zz}}{3} \qquad (6)$$

The proportion of the total mean stress transmitted by the finer fraction, α_f, is calculated as p^f/p, and similarly, the proportion of the total mean stress transmitted by the coarser fraction, $\alpha_c = 1 - \alpha_f$, is calculated as p^c/p, where p^f and p^c are the mean stress transmitted by the finer and the coarser populations, respectively.

Fig. 9 shows the evolution of the α_f during shearing for the dense and loose assemblies of binary mixtures[10]. The α_f for the dense assemblies having $f_c \geq 30\%$ decreased significantly (with more pronounced decrease observed for $35\% \leq f_c \leq 50\%$ which corresponds with regime 2 in Table 3) from the start of shearing until $\epsilon_a \approx 0.08$ beyond which the change in the α_f became minimal (Fig. 9a). α_f for the loose assemblies generally exhibited minimal changes from the start to the end of shearing (Fig. 9b). In agreement with the data presented by Sufian et al., (2021) for sand-silt mixtures subjected to constant mean stress triaxial compression, the

[9] Note that σ_{ij}^c and σ_{ij}^f correspond to the contribution of coarse and fine particles to the total stress and not to the mean stress in coarse and fine particles. To compute the stress in the coarse particles, we consider both the coarse-coarse and the coarse-fine contacts. Similarly, to compute the stress in the fine particles, we consider both the fine-fine and the coarse-fine contacts.

[10] In Appendix B and Fig. A2, we show that the evolution of the deviatoric stress transmitted by the fines is generally similar to the evolution of the mean stress presented in Fig. 8.

observation made here indicates the transmission of stresses from the fine particles to the coarse particles or a concentration of stress on the coarse particles, in the dense assemblies, at the early stage of shearing. This phenomenon occurred such that for each f_c, a unique α_f exists for both the initially dense and loose assemblies at large strains (i.e. at the critical state).

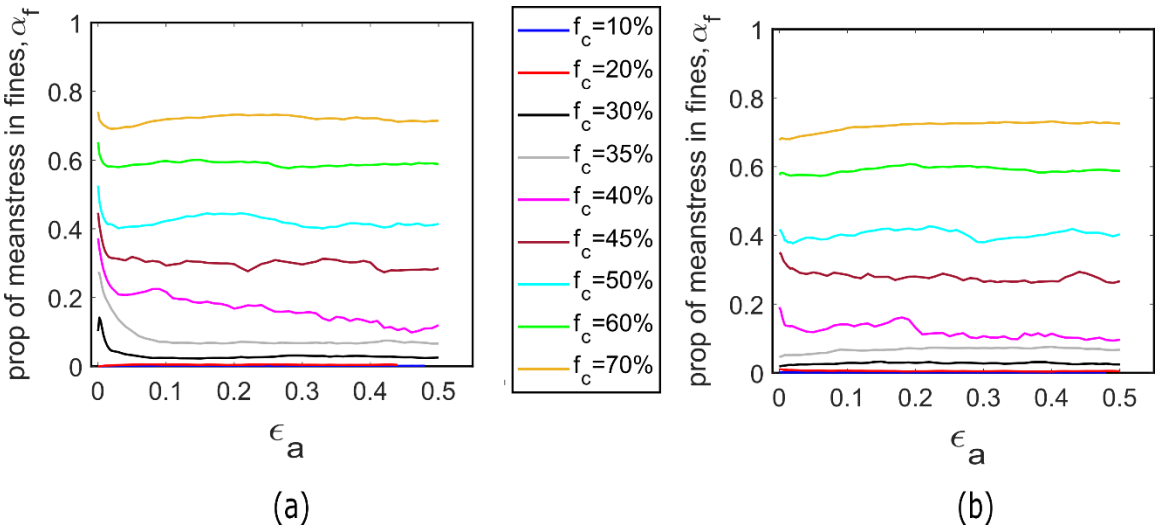

Fig. 9 Evolution of the proportion of mean stress transmitted by the fines during shearing for (a) dense assemblies (b) loose assemblies[11]

Fig. 10 shows the contribution of the finer fraction, α_f, and the coarser fraction, α_c, to the total mean stress for the studied assemblies. At all stages of shearing considered (Fig. 10a-d), the fine particles did not contribute to stress transmission (i.e. $\alpha_f \approx 0$) until the f_c^{th} beyond which there was a progressive increase in the α_f and a consequential reduction in α_c. The primary stress-transmitting skeleton at $f_c < f_c^{th}$ is therefore the coarser fraction. Based on a conceptual analysis proposed in the experimental studies on granular mixtures (Thevanayagam et al., 2002; Thevanayagam & Mohan, 2000), the mechanical behaviour of the mixtures should be primarily controlled by the fines at $f_c \geq f_c^{th}$. Vallejo (2001) in his experimental study on binary granular mixtures suggests that at f_c>60%, the fines generally become the primary stress-transmitting matrix while the coarser fraction plays basically no role in stress transmission. The evidence from our micromechanical analysis shows that while the fines began to transmit stress at the f_c^{th}, they did not become the primary stress-transmitting fabric until f_c becomes higher than an equivalent fines content f_c^{eq}. Here, f_c^{eq} is the estimated f_c at which the total mean

[11] By comparing the q/p data (Figs. 3 & 4) with the α_f data (Fig. 9), it is observed that the fluctuation in the q/p data for the assemblies having $f_c \in [30\% ; 40\%]$ is not reflected in the relatively smooth α_f data. This is because the fluctuations evident in the q/p data is masked behind the apparently smooth α_f data as a result of the normalisation of the stress transmitted by the fines with the total mean stress (p^f/p).

pressure is equally shared between the finer and the coarser fraction. For the studied binary mixtures, f_c^{eq} is estimated to range from 48% to 53% for the dense assemblies at the initial state and the peak; and reaches 55% for the loose assemblies at the initial state and for all assemblies at the critical state. Contrary to Vallejo (2001), while the fines transmit the largest fraction of the total mean stress for $f_c > f_c^{eq}$, the coarse particles continue to make a secondary and yet significant contribution to the total mean stress for much larger fine contents (at least up to f_c=70% studied here).

Since particles stresses result from contact forces, we estimate in Fig. 11, the proportion of the total number contacts shared by the fines[12], C_n^f, and the coarse particles, C_n^c. Comparing these geometric statistics to the stress contributions enables a better understanding of the trends observed in Fig. 10. Again, the trends in Fig. 11 can be classified into two regimes delineated by the threshold fines content, f_c^{th}. For $f_c < f_c^{th}$, C_n^f generally increased with f_c but remained lower than C_n^c, indicating that in this regime, the coarse particles are involved in a larger proportion of the total number of contacts than the fines. For $f_c \geq f_c^{th}$, C_n^f increased monotonically with f_c and was higher than C_n^c; in this case, the fines became dominant in terms of their proportion of the total number of contacts. By comparing Fig. 10 and 11, we observe that although the fines became dominant in terms of their proportion of the total number of contacts from $f_c = f_c^{th}$, they did not primarily contribute to the total mean stress until $f_c > f_c^{eq}$. This indicates that most of the contacts involving fine grains do not carry large forces for $f_c^{th} < f_c < f_c^{eq}$.

[12] The contacts made by the coarse particles include both the coarse-coarse and the coarse-fine contacts while the contacts made by the fine particles include both the fine-fine and the coarse-fine contacts. The proportion of the total number of contacts shared by the fines, C_n^f, is calculated as: $C_n^f = \frac{2N_{f-f}+N_{c-f}}{2N_{f-f}+2N_{c-f}+2N_{c-c}}$.

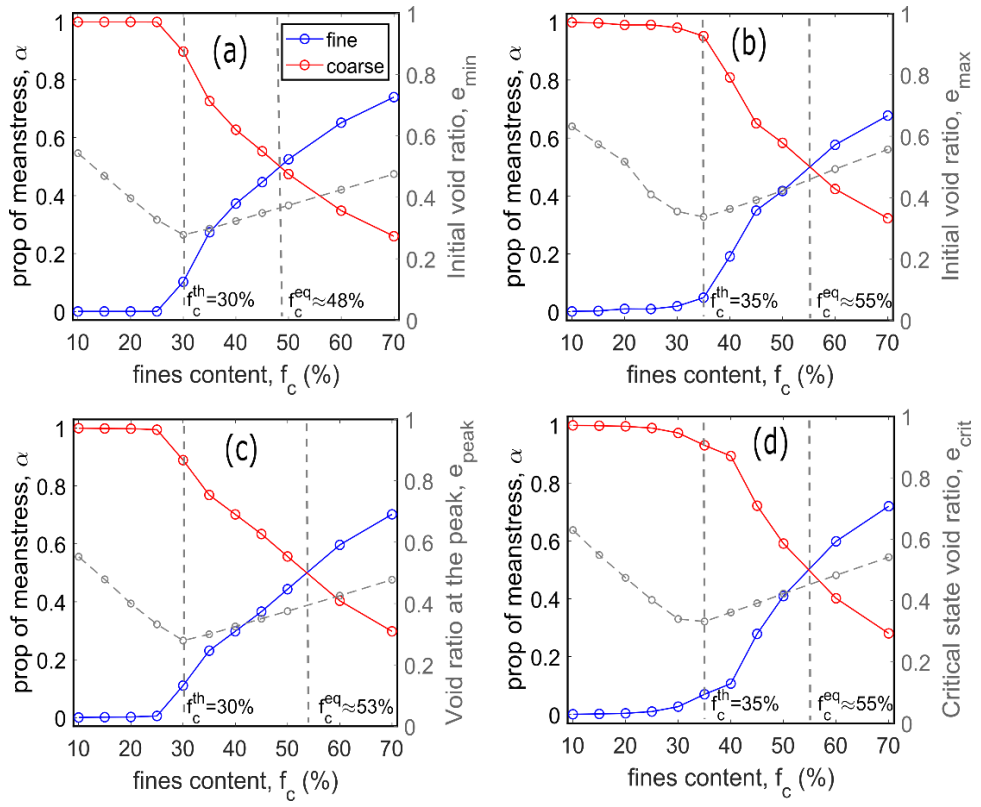

Fig. 10 Proportion of mean stress transmitted by the fines and coarse particles at (a) the initial state for dense assemblies (b) the initial state for the loose assemblies (c) the peak (d) the critical state (unique trends for both dense and loose assemblies)

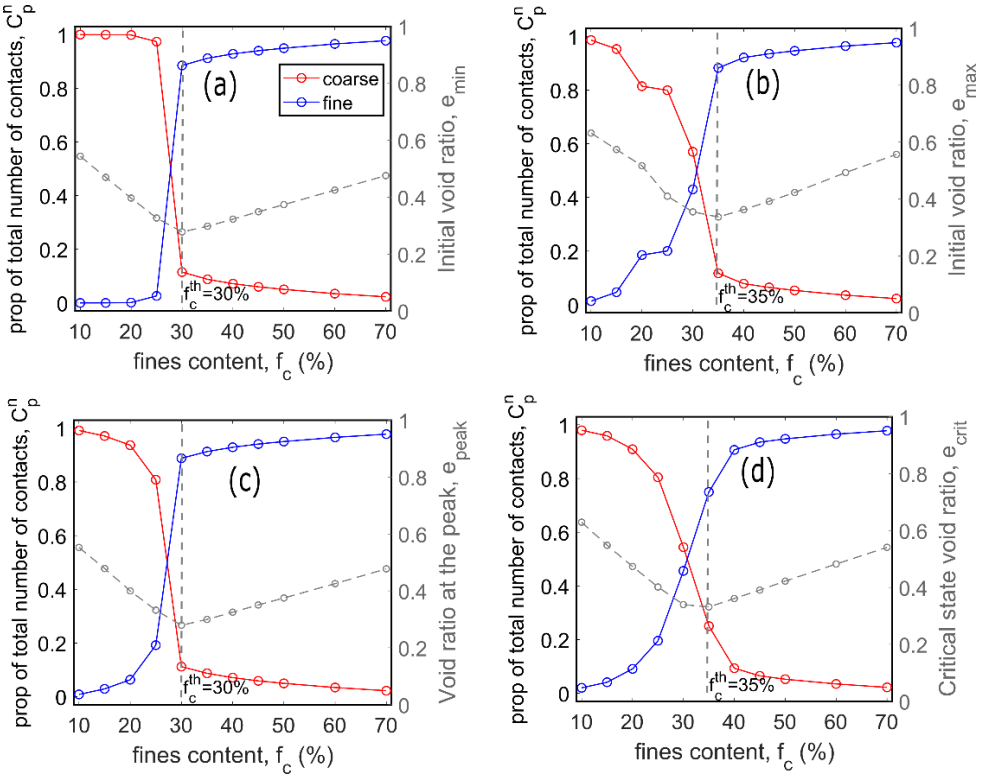

Fig. 11 Proportion of the total contacts belonging to the finer and coarser fraction at (a) the initial state for dense assemblies (b) the initial state for the loose assemblies (c) the peak (d) the critical state (unique trends for both dense and loose assemblies)

Figs. 12 and 13 show the cumulative distributions of the individual stresses sustained by the particles normalised by the average particle stresses in the whole assembly ($P^p/\overline{P^p}$), for the coarser and finer fraction respectively, at the initial states, the peak and the critical state. This is aimed at understanding the range and state of particle stresses existing within the particle size fractions in each assembly at different shearing stages. A wider range of stresses exist within the finer fraction (Fig. 13) than the coarser fraction (Fig. 12). For the coarser fraction, the proportion of the particles with stress values below the average stress (i.e. $P^p/\overline{P^p} \leq 1$) was similar for all f_c values considered. Below the average stress, the cumulative distribution shifts to the right as f_c increased; the reverse was observed above the average stress. The width of the distributions for the coarser fraction tend to become smaller as f_c increased (Fig. 12a-d). This indicates a more even stress distribution within the coarser particles as f_c increased. The proportion of the fines with stress values below the average (i.e. $P^p/\overline{P^p} \leq 1$) decreased as f_c increased (Fig. 13).

The proportion of the fines bearing no stress (i.e. $P^p/\overline{P^p} = 0$), referred to as the non-active fines, R_f, are illustrated by the vertical line at $P^p/\overline{P^p} = 0$ in Fig. 13 and are plotted in Fig. 14a. Fig. 14b shows the change in the percentage of the non-active fines present within the assemblies during shearing, ΔR_f (i.e. the difference in the R_f at the initial states and the critical state). Within the assemblies having $f_c < f_c^{th}$, virtually all the fines (98.3% to 99.9%) are non-active. This confirms that at $f_c < f_c^{th}$, the finer fraction does not contribute to stress transfer. For $f_c^{th} < f_c < 45\%$, R_f decreases more significantly than for $f_c > 45\%$ (Fig. 14a). The drop in the proportion of non-active fine (within $f_c^{th} < f_c < 45\%$) depends significantly on the relative density of the assemblies (dense or loose) and the stage of shearing (initial, peak or critical state). Three regimes are identified following the analysis here. For $f_c < f_c^{th}$, the fines are largely dormant whatever the sample state[13]. Also, $\Delta R_f \approx 0$ (Fig. 14b), indicating shearing had no effect on the activity of the fines. For $f_c^{th} \leq f_c < 45\%$, the proportion of active fines is very sensitive to the packing density and the stage of shearing (Fig. 14a). Also, ΔR_f is highest (Fig. 14b), suggesting that more of the active fines initially present within the assemblies became non-active by the end of shearing (38%-85% and 11-12% for dense and loose assemblies, respectively). For $f_c \geq 45\%$, the proportion of non-active fines is rather low and exhibit a limited sensitivity to the packing density and the stage of shearing.

[13] Note that, depending on the sample preparation procedure, we could imagine having fewer non-active fines at initial state. This is for instance the case when samples are prepared in the lab using the moist tamping method that gather fines around contacts between coarse grains because of capillary effects.

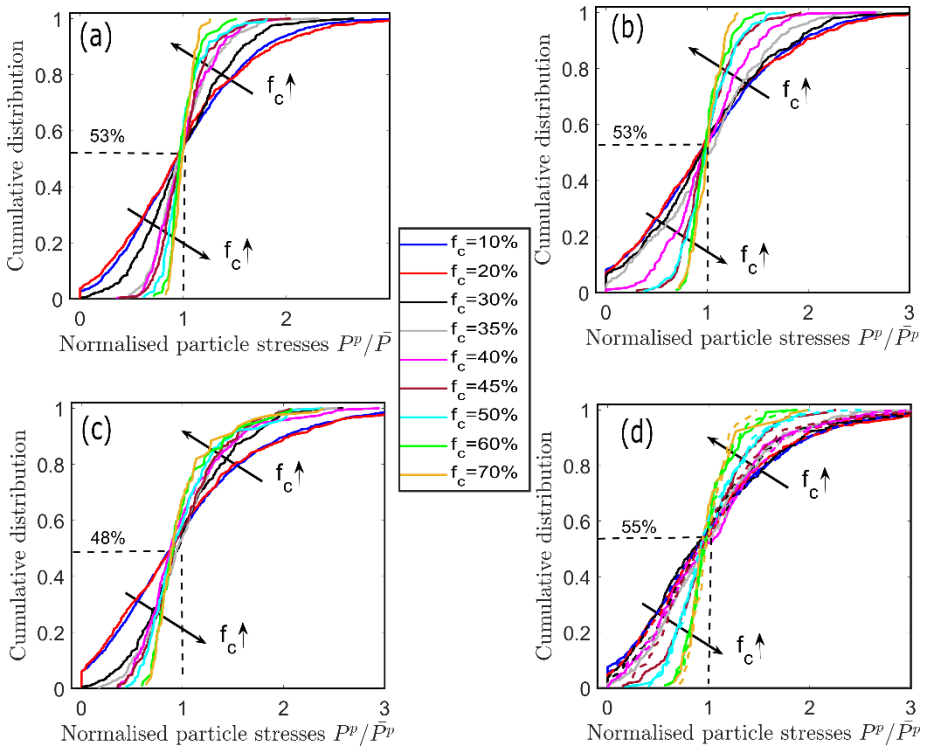

Fig. 12 Cumulative distribution of normalised particle mean stress for coarser fraction (a) dense; initial state (b) loose; initial state (c) dense; peak state (d) critical state for both dense (solid line) and loose (dashed line) assemblies

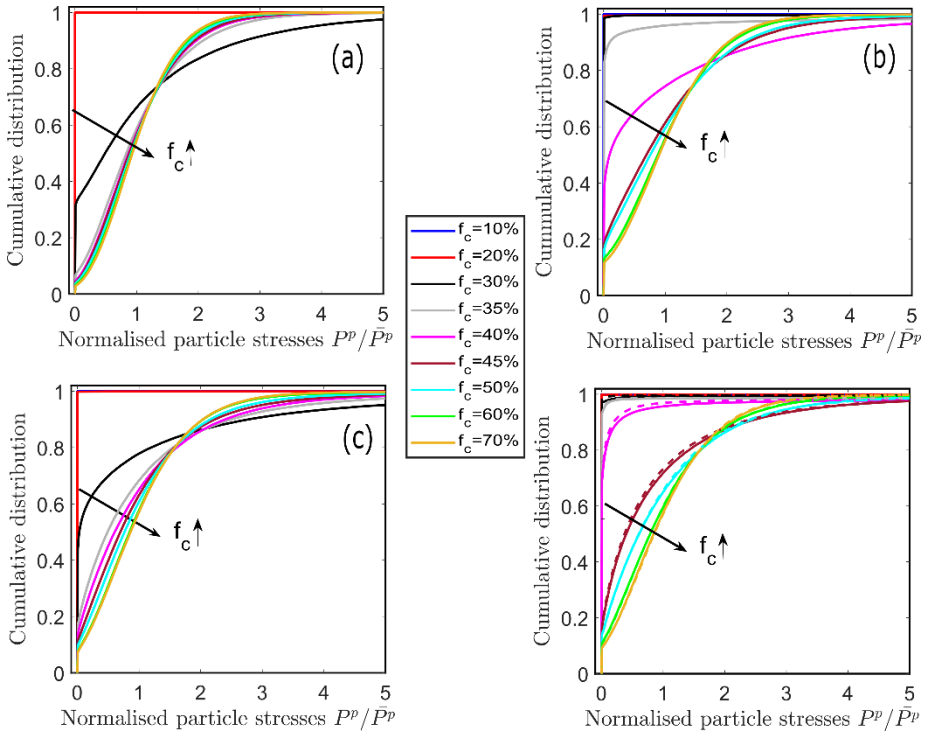

Fig. 13 Cumulative distribution of normalised particle mean stress for finer fraction (a) dense; initial state (b) loose; initial state (c) dense; peak state (d) critical state for both dense (solid line) and loose (dashed line) assemblies

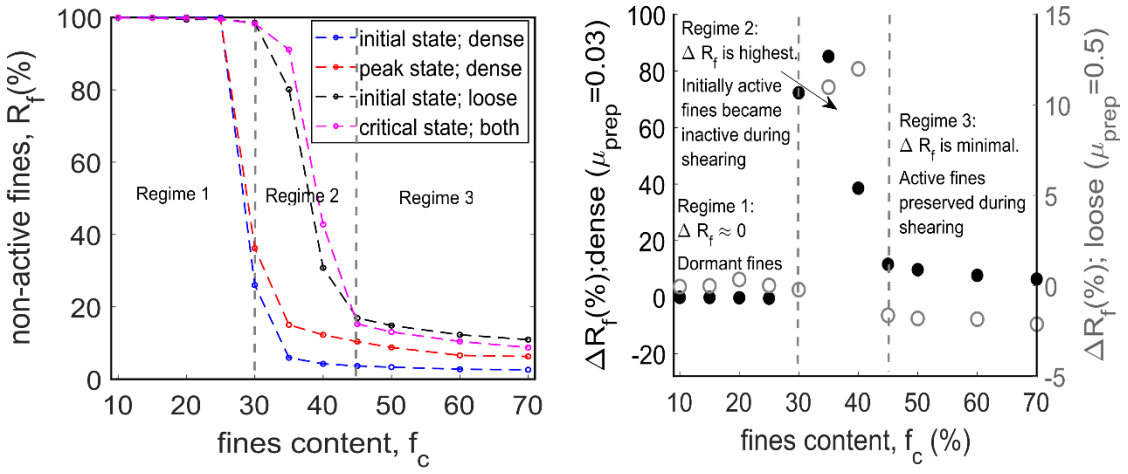

Fig. 14 (a) Percentage of non-active fines, R_f, at different f_c (b) Change in the percentage of non-active fines during shearing (filled circle for dense assemblies and open circles for loose assemblies). ΔR_f>0 and ΔR_f<0 mean higher and lower percentages of inactive fines at the end of shearing in comparison to the initial state, respectively.

5. Contact based stress-transmission

Using the Love-Weber contact based stress tensor including Bagi boundary term (Bagi, 1999), the contributions of all contact types to the total mean stress transmitted by an entire granular system is given as:

$$\sigma_{ij}^{c} = \frac{1}{V}\sum_{c=1}^{N_c} f_j^c \, l_i \qquad (11)$$

where N_c is the total number of contacts in the granular system, V is the volume of the system, $\boldsymbol{l}$ is the branch vector ($\|\boldsymbol{l}\| = R_1 + R_2$ for a sphere 1 to sphere 2 contact; $\|l\| = R_p$ for a sphere p to wall contact), and $\boldsymbol{f^c}$ is the contact force vector. This stress tensor can be decomposed based on the contact type as:

$$\sigma_{ij}^{k} = \frac{1}{V}\sum_{c=1}^{N_c^k} f_j^c \, l_i \qquad (12)$$

where k ∈ {c-c, c-f, f-f, s-wl}. c-c, c-f, f-f, and s-wl denote coarse to coarse, coarse to fine, fine to fine and sphere to wall contacts, respectively. The proportion of the total mean stress from each contact type is given by $\alpha_k = p^k/p$. Note that the boundary term is expected to vanish as soon as the sample domain is sufficiently large (which should be the case when the REV condition is met).

Fig. 15 shows the evolution of the proportion of the stress transmitted by each contact type during shearing, for the dense and loose assemblies. At large strains (i.e., ϵ_a >0.3), the contribution of the coarse to coarse contacts to the total mean stress, α_{c-c}, decreases with f_c such that α_{c-c} ≈0 for f_c > 40% (Fig. 15a&d). The contribution of the fine-fine contacts to the total mean stress, α_{f-f}, increases with f_c for f_c>f_c^{th} while α_{f-f} ≈0 for f_c<f_c^{th} (Fig. 15c&f). The contribution of the coarse to fine contacts, α_{c-f}, initially increases with f_c until f_c=40% and thereafter decreases with further increase in f_c (Fig. 15b&e). During the early stage of shearing (i.e., $\epsilon_a < 0.1$), we observed a decrease in α_{c-c} and α_{f-f} which is accompanied by a commensurate increase in the α_{c-f}. This indicates a redistribution of stress from the c-c and f-f contacts to the c-f contacts. Although the coarse particles lost stress as indicated in the decrease in α_{c-c}, they are also gained stress from the fines as indicated in both the increase in α_{c-f} and the decrease in α_{f-f}. Ultimately, there was a redistribution of stress from the fines to the coarse particles as indicated in Fig. 9a.

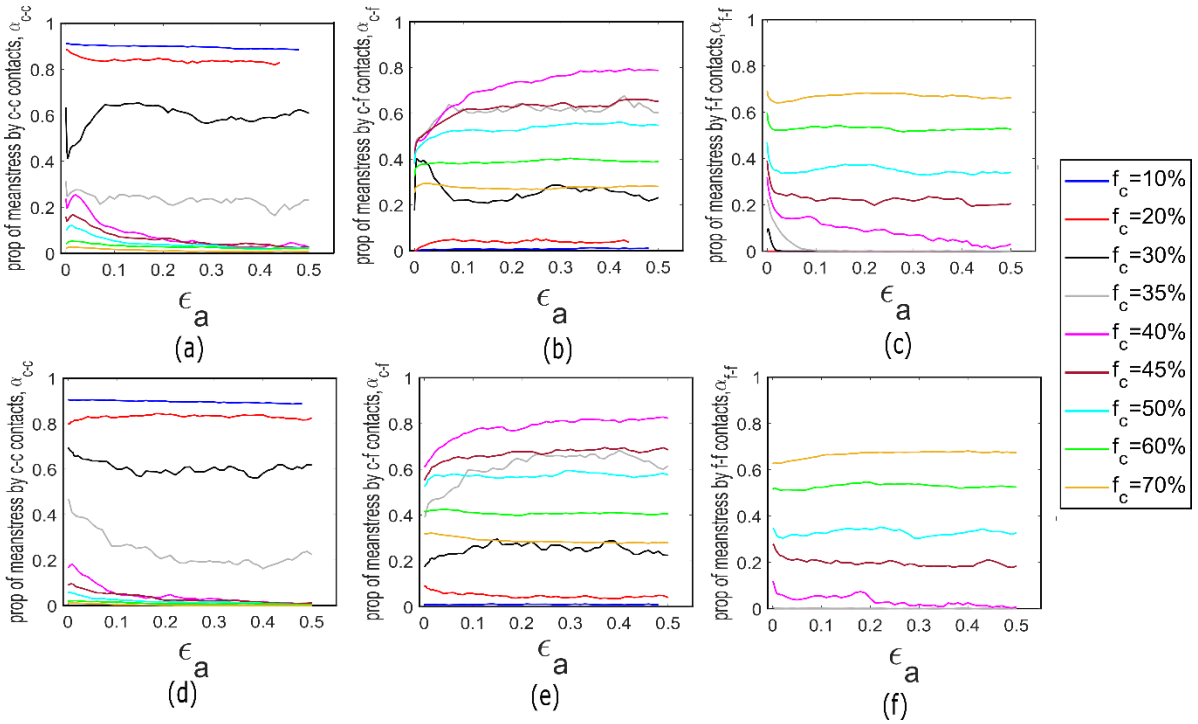

Fig. 15 Evolution of the proportion of mean stress transmitted by contact types during shearing for (a) c-c contacts; dense (b) c-f contacts; dense (c) f-f contacts; dense (d) c-c contacts; loose (b) c-f contacts; loose (c) f-f contacts; loose

Fig. 16 shows the proportion of the mean stress transmitted by each contact types at the initial states, the peak and the critical state. The trends observed between the contact types[14] can be classified into four regimes based on the f_c. In the first regime (f_c<f_c^{th}), the contribution of the fine to fine contacts to the total mean stress, α_{f-f}≈0, indicating that the f-f contacts do not contribute to mean stress below the f_c^{th}. In this regime, the condition $\alpha_{c-c} > \alpha_{c-f} > \alpha_{f-f}$ generally holds, hence, the regime is referred to as coarse-dominated, following Vallejo (2001) and Sufian et al. (2021). Within the second regime referred to as transitional coarse-dominated (f_c^{th}<f_c<f_c^{tr}, where f_c^{tr} is referred here as transitional fines content where α_{c-c}=α_{f-f}), the condition $\alpha_{c-f} > \alpha_{c-c} > \alpha_{f-f}$ generally holds. In the third regime where f_c^{tr}<f_c<f_c^{eq} (f_c^{eq} was defined in Section 4 as the f_c at which the total mean stress is equally shared between the coarser and the finer fractions) and referred to as transitional fines-dominated, the condition $\alpha_{c-f} > \alpha_{f-f} > \alpha_{c-c}$ holds. The transitional fines content, f_c^{tr}, delineating the transitional regimes (i.e. the transitional-coarse dominated and the transitional-fines dominated regimes) was found around f_c = 40% for the assemblies and the shearing stages considered here (Fig. 16a-d). The transitional regime based on the micromechanical analysis ranged from f_c^{th} to f_c^{eq} and is therefore within f_c=30%-48% and f_c=35%-55% for the dense and loose assemblies, respectively. For f_c>f_c^{eq} (i.e., in the fourth regime), the condition $\alpha_{f-f} > \alpha_{c-f} > \alpha_{c-c}$ holds, hence, the regime is fines-dominated. While the classification in the experimental study by Vallejo (2001) was based on void ratio, we present here a similar classification based on the micromechanical analysis conducted, with distinct delineations in agreement with the 3-D DEM study on binary mixtures having size ratio, λ=4, reported by Minh et al., (2014).

[14] Excluding the contributions to the mean stress from the contacts between the spherical particles and the walls, α_{s-wl}, which were generally less than 0.15. We observed that α_{s-wl} values for the underfilled assemblies (f_c<f_c^{th}) were generally higher than the overfilled assemblies. This suggests that a greater number of particles is required to ensure a representative element volume (REV) in underfilled assemblies in comparison to the overfilled assemblies.

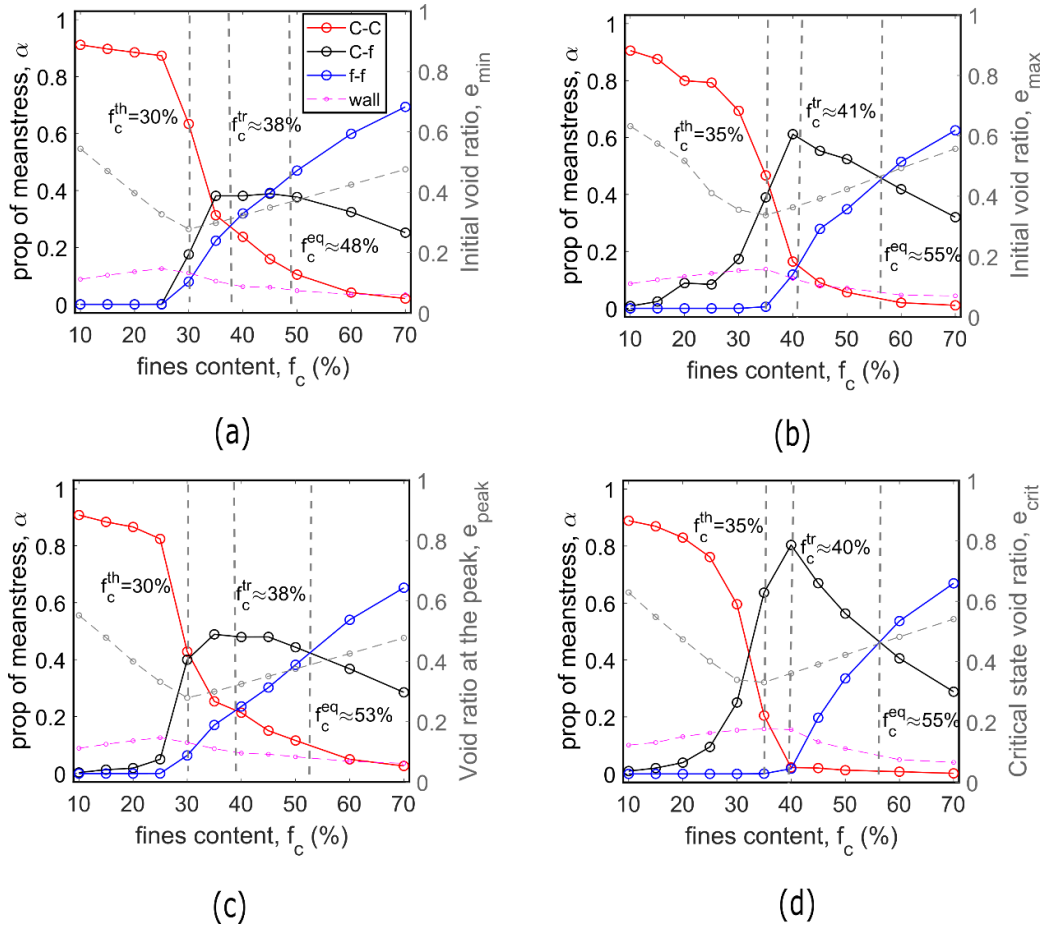

Fig. 16 Proportion of mean stress transmitted by contact type at (a) the initial state for dense assemblies b) the initial state for the loose assemblies (c) at the peak (d) the critical state (unique trends for both dense and loose assemblies). Void ratio data represented with dashed grey lines are plotted on the right side of each subplot to help identify the different regimes.

In a similar fashion to Fig. 11, Fig. 17 shows the proportion of all contacts belonging to each contact types at the different stages of shearing. The trends between the contact types here could be generally grouped into two categories delineated by the threshold fines content[15].

- For $f_c<f_c^{th}$, the proportions of the total contacts belonging to the f-f contacts, C_{f-f}^t, were lower than those belonging to the c-c contacts, C_{c-c}^t. The condition, $C_{c-c}^t > C_{c-f}^t > C_{f-f}^t$ generally holds, except for f_c=30% in the loose samples (Fig. 17b) and at the critical state (Fig. 17d) where the condition $C_{c-f}^t > C_{c-c}^t > C_{f-f}^t$ holds.
- For $f_c \geq f_c^{th}$, the f-f contacts dominate the assemblies, therefore the condition $C_{f-f}^t > C_{c-f}^t > C_{c-c}^t$ holds.

[15] The proportions of all contact types belonging to the wall, C_{wl}^t were less than 0.17 and 0.08 for $f_c<f_c^{th}$ and for $f_c>f_c^{th}$, respectively.

From the threshold fines content, the C_{c-c}^{t} values were significantly low (ranging from 2.1e-2 – 9e-5) at all states, and was zero for f_c=70% at the critical state (Fig. 17d). This show that the fines disperse the coarse particles (i.e. C_{c-c}^{t} becomes minimal) from the threshold fines content, f_c^{th}, which is in agreement with the 3D DEM study on binary mixtures by Minh et al., (2014), and not beyond f_c^{th} as suggested in the experimental study on sandy-gravels by Skempton & Brogan (1994). The suggestion by Salgado et al., (2000) in their experimental study, that the fines controls the mechanical behaviour of sand-silt mixtures when the sand particles are completely floating ($C_{c-c}^{t} \approx 0$) in the silts is not supported by the data shown here. While the fines disperse the coarse particles from f_c^{th}, they did not become the primary stress-transmitting matrix until f_c^{eq} is reached as explained in Section 4. In the transitional regime, there is the possibility that some fines get trapped between the coarse particles while being loosely connected to the rest of the fines in the assemblies.

Also, while for $f_c<f_c^{th}$, the $C_{c-f}^{t} \approx 0$ in the dense assemblies (Fig. 17a), in the loose assemblies (Fig. 17b), $C_{c-f}^{t}>0$. This suggests that, in agreement with Thevanayagam et al., (2002) and Shire, (2014), the fines in the dense assemblies are confined within the voids between the coarse particles with little interaction with the coarse matrix; in the loose assemblies, the fines interact more with the coarse particles. The fact that the fines are interacting more with the coarse particles in the loose case may indicate the fines are trapped within the coarse particles thereby creating larger voids which may require more fines to fill in comparison to the dense assemblies. This observation is consistent with Salgado et al., (2000) and Lade & Yamamuro (1997) who found more fines on the surfaces of the coarse particles in their loose assemblies, in comparison to the dense assemblies, and suggested that this is responsible for the larger drop in the e_{min} than in the e_{max} for a given increase in the fines content. The drop in the e_{max} is mitigated than in the e_{min} because the fines interacting with the coarse particles helps to create larger voids hence the lower drop in the void ratio in the loose case.

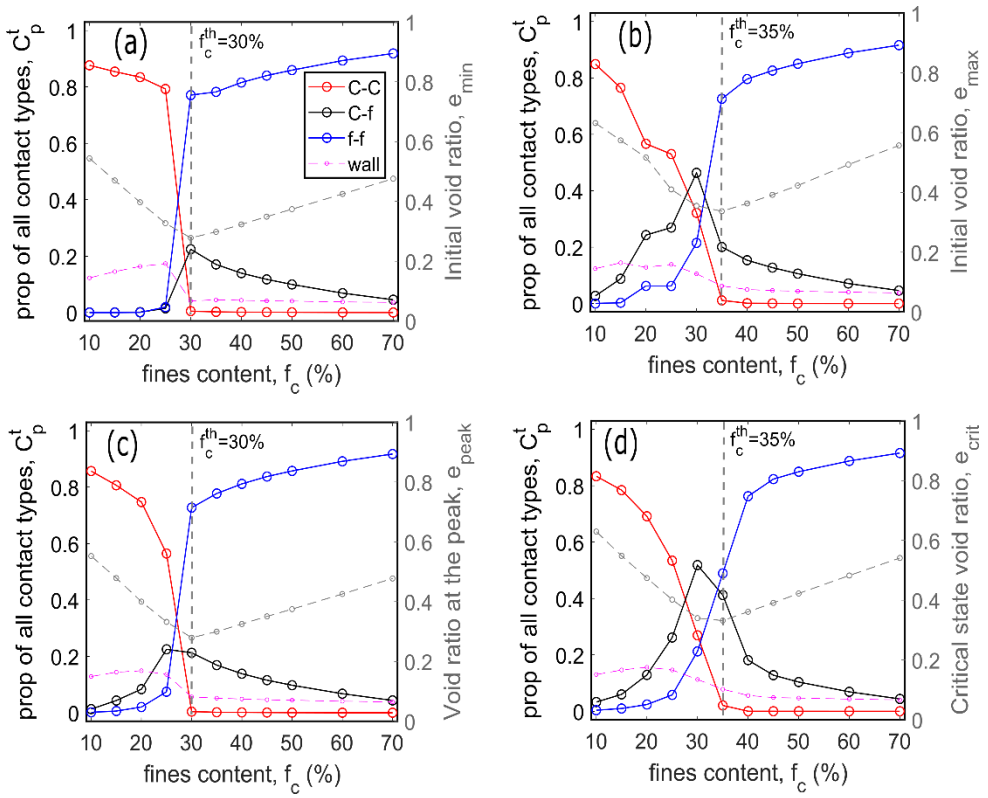

Fig. 17 Proportion of the total contacts belonging to each category of contact type at (a) the initial state for dense assemblies (b) the initial state for the loose assemblies (c) the peak (d) the critical state (unique trends for both dense and loose assemblies). Void ratio data represented with dashed grey lines are plotted on the right side of each subplot to help identify the different regimes.

6. Stress-based skeleton void ratio

The idea of sand skeleton void ratio was introduced in the experimental study by Kuerbis (1989) in order to understand the behaviour of silty sands with various fines content under undrained triaxial shearing. This proposition, which was based on a conceptual analysis of the fabric of soil mixtures, have been applied in other experimental and numerical studies (Benahmed et al., 2015; Chang & Yin, 2011; Lade & Yamamuro, 1997; Ni et al., 2004; Pitman et al., 1994; Rahman et al., 2008; Thevanayagam, 1998; Thevanayagam et al., 2002; Vaid, 1994). In order to understand the critical state behaviour of the gap-graded assemblies subjected to drained shearing in this study, we propose a skeleton void ratio based on the stress sustained by individual particles. The skeleton void ratio, e_{skel}, is here defined as the void ratio of a granular system when the fines with particle stress, P^p, lower than a threshold stress value are regarded as part of the void space and are therefore excluded. Note that we propose to exclude only the fines (and not the coarse particles) for our skeleton void ratio calculation. This is based on the fact that loosely stressed fine particles may be eroded through the constrictions

of the soil matrix whereas coarse particles cannot as they are usually larger than the constriction size (Garner & Fannin, 2010; ICOLD, 2017; A. W. Skempton & Brogan, 1994; Thevanayagam & Mohan, 2000). In Figure 17 we show the variation of the proportion of the total mean stress transmitted by the "skeleton" finer fraction, α_f^{skel}, for different stress thresholds, where the threshold stress is defined as:

$$\text{Threshold stress} = \underbrace{x}_{\substack{\text{threshold} \\ \text{coefficient}}} \times \underbrace{\overline{P^p}}_{\substack{\text{Average} \\ \text{particle stress}}} \quad (10)$$

In Fig. 18, the threshold coefficient, x, ranges from 0 to 2.

- Unsurprisingly, the contribution of the fine remains negligible whatever the threshold value for $f_c<f_c^{th}$ (the contribution for all the fines, α_f, is already negligible).
- For $f_c^{th} \leq f_c \leq 45\%$, generally no change is observed in α_f^{skel} until $x = 0.1$, which means that the fine grains transmitting a pressure P^p lower than 10% of the mean pressure $\overline{P^p}$, contribute only marginally to the stress transmitted by the finer fraction.
- For f_c>45%, no change was observed in α_f^{skel} until $x > 0.25$.

From the above analysis, we can retain x=0.1 as a reasonable threshold to define the skeleton fines for all fines content.

Fig. 19 shows the proportion of the fines left in an assembly after each exclusion. These "skeleton" fines are included in the solid volume while computing the stress-based skeleton void ratio, e_{skel} plotted in Fig. 20. For $f_c \geq f_c^{th}$, the proportion of the fines included as part of the assembly skeleton decreases monotonically as the threshold stress increases (Fig. 19a-d).

The mechanical void ratio, e_{mech} has been computed in the literature as an alternative void ratio index to the void ratio, e, of granular materials (Liu et al., 2022; Otsubo, 2016). e_{mech} excludes the particles with $c \leq 1$. In Fig. 20, we compare the evolutions of e, e_{mech} and e_{skel} (for $x = 0.1$), $e_{skel}; x = 0.1$, for the different fines contents. These evolutions are put in parallel with the peak and the critical state stress ratios.

As shown in Figure 19, $e_{skel}; x = 0.1$, shows a negative correlation with the critical state strength, $(q/p)_{crit}$ (Fig. 20b & d), and no correlation with the peak strength, $(q/p)_{max}$ (Fig. 20a). Instead, at the peak, $(q/p)_{max}$ correlates negatively with e, (Fig. 20a & c), in agreement with established relationship between the initial void ratio and the peak strength in the literature (Adesina et al., 2023; Holubec & D'Appolonia, 1973; Ng, 2004). In order to determine the best performing void ratio index among the indexes considered here, we estimated the goodness of the fit, R^2, for the relationship between the void ratio values determined using the indexes and the strength exhibited by the assemblies (Table A.1 in the Appendix C). It is obvious that

$e_{skel}; x = 0.1$ provides the best fit (R^2=0.84) thereby yielding the best prediction of $(q/p)_{crit}$, while the best performing void ratio index for $(q/p)_{max}$ is e (R^2=0.90 for underfilled and R^2=0.97 for the overfilled assemblies). This finding is consistent with the fact that the microstructure of granular assemblies (including the force chain network) evolve rapidly under shearing at the critical state (Deng et al., 2022; Wautier et al., 2018). Consequently, the non-active and the marginally active fines do not have the chance to interact with the force chains and should therefore not be considered as part of the void when assessing the mechanical behaviour. On the contrary, at the peak, although the non-active and the marginally active fines do not contribute significantly to the total mean stress, they serve as a support for the force chain network and as a result constitute an important part of the microstructure of the assemblies (Tordesillas et al., 2010; Wautier et al., 2018; Zhu et al., 2016a; Zhu et al., 2016b). Therefore, they have to be taken into account in the void ratio calculation.

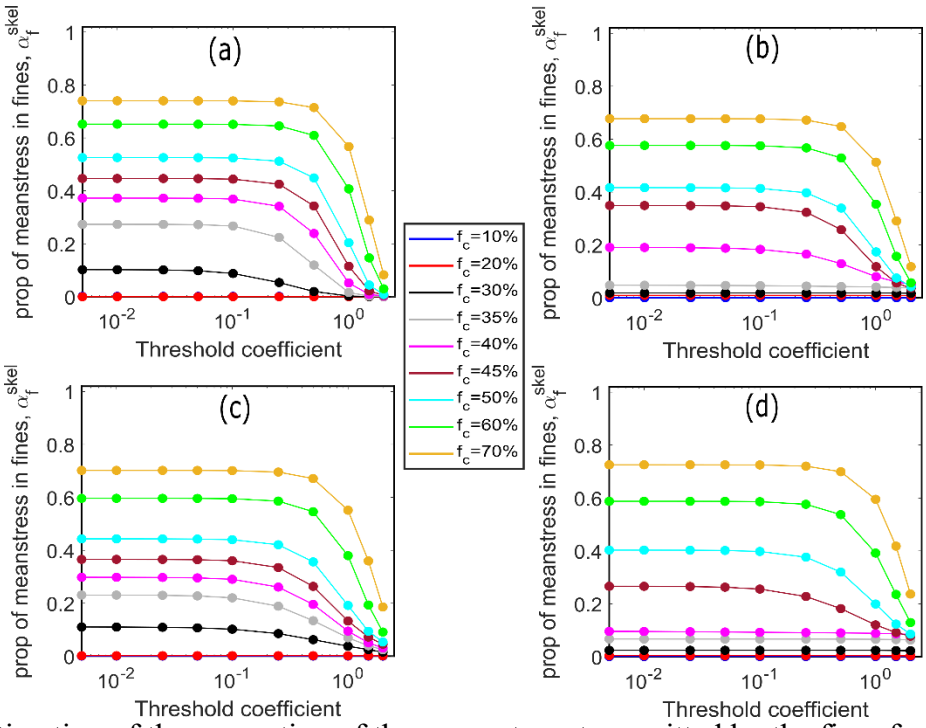

Fig. 18 Estimation of the proportion of the mean stress transmitted by the finer fraction when particles with particle stress lower than a threshold are excluded (a) dense; initial state (b) loose; initial state (c) dense; peak state (d) critical state (unique trends for both dense and loose assemblies)

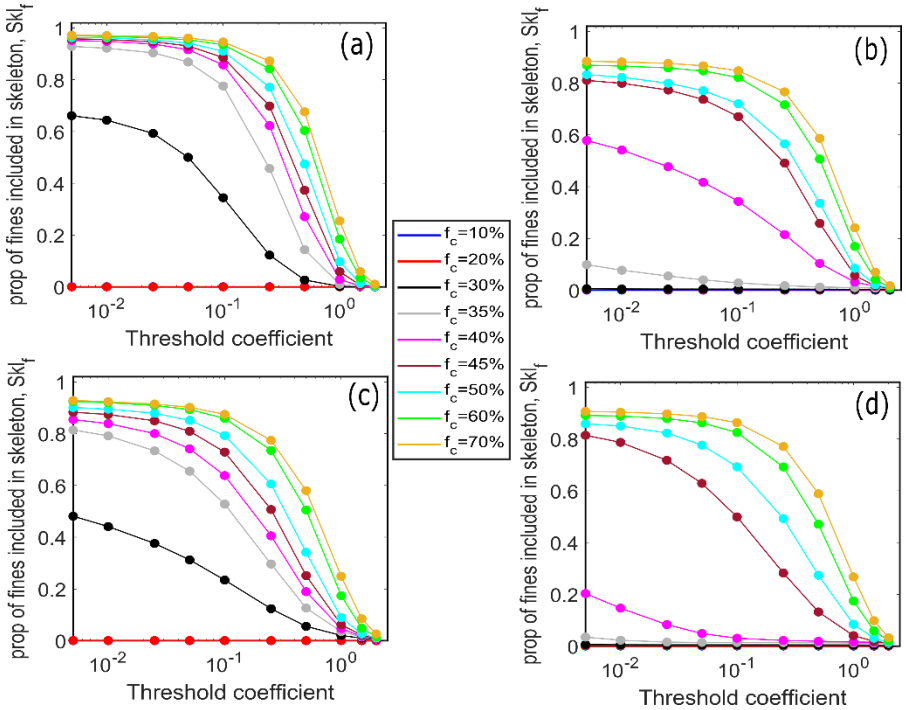

Fig. 19 Proportion of skeleton fines as a function of the threshold coefficient (a) dense; initial state (b) loose; initial state (c) dense; peak state (d) critical state (unique trends for both dense and loose assemblies)

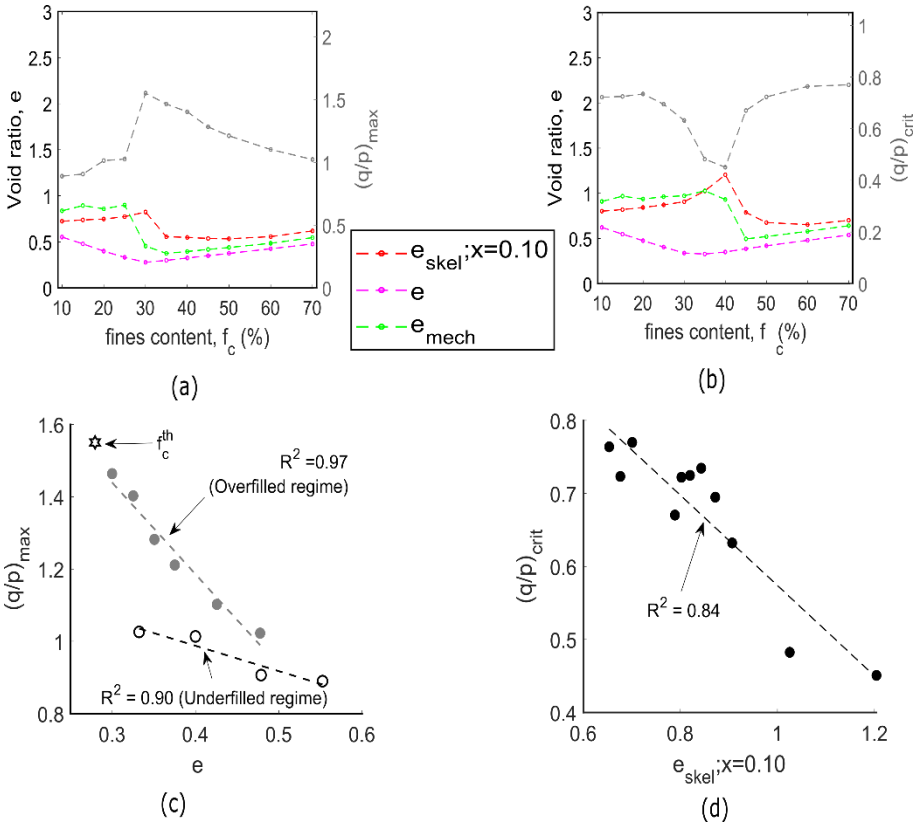

Fig. 20 (a) void ratio indexes at the peak and $(q/p)_{max}$ (b) void ratio indexes at the critical state and $(q/p)_{crit}$, for different f_c values. Relationship between (c) e and $(q/p)_{max}$ (d) e_{skel};x=0.1 and $(q/p)_{crit}$.

7. Summary and Conclusions

This study presents a micromechanical evaluation of the regimes delineating the behaviour of gap-graded granular assemblies of different fines content, using discrete element simulations. The existence of the regimes delineated by milestone fines content was assessed using the macromechanical and micromechanical characteristics of the assemblies, and the contributions of the particle size fractions and contact types to the total mean stress. The key findings and conclusions are presented below.

(i) Two regimes were identified based on the macroscopic characteristics of the assemblies, three regimes based on particle scale analysis and four regimes based on contact scale analysis. We provide distinct delineations of the regimes by fines content, in an original manner. Fig. 21 presents a summary of all the regimes identified in this study. Table 3 highlights the unique trends characterising the three regimes identified based on the macromechanical and the micromechanical analyses conducted. We showed that the boundaries delineating the identified regimes depend on density and stress state. We acknowledge that the boundaries can also vary with a change in particle size ratio (and more generally a change in coarse and fine particle size distributions) which is beyond the scope of our study.

(ii) The micromechanical analyses adopted overcome the limitation of experimental studies where it is difficult to ascertain the claims emanating from the conceptual analysis presented in the studies, since individual particles stresses or particle dispersion cannot be easily determined in experiments. The claims that the fines become the primary stress-transmitting matrix at the threshold fines content or at a limiting fines content; or that stress is equally sheared by the coarse and the fine particles in the transitional zone (Vallejo, 2001) or at f_c>35% (Shire et al., 2014) are not supported by the evidence provided here. Instead, we found that the coarse particles are dispersed by the fines (i.e. where coarse to coarse contacts are minimal or non-existent) from the threshold fines content. In addition, the fines do not contribute to the total mean stress below the threshold fines content, they play a secondary role in the transitional zone ($f_c \in [30\% ; 55\%]$ depending on density and stress state), and only become the primary stress-transmitting matrix beyond the transitional zone (i.e. when $f_c > f_c^{eq}$; $f_c^{eq} \in [48\% ; 55\%]$ depending on density and stress state).

(iii) We found that the threshold stress which determines whether a fine particle transmits a marginal or a significant stress with respect to the contribution of the fines to the total mean stress is a fraction of the average particle stress, $\overline{P^p}$, within an assembly; where the threshold stress values are $0.1 \times \overline{P^p}$ for $f_c^{th} \leq f_c \leq 45\%$, and $0.25 \times \overline{P^p}$ for f_c>45%. The threshold stress concept proposed in this study can be useful in determining the particles that constitute important mesostructures (i.e. important force-chain networks) in gap-graded granular assemblies. The skeleton void ratio determined based on the threshold stress correlates with the critical state strength of the assemblies, while no correlation was found between the critical state strength and alternative void ratio indexes such as the void ratio and the mechanical void ratio at the critical state. The marginal stress transmitting fines (marginally active fines) determined based on the threshold stress may constitute a part of the particles susceptible to internal erosion, in addition to the non-inactive fines in a gap-graded assembly (particles with zero or only one contact).

In addition to the standard underfilled and overfilled regimes, future DEM studies could focus on the two transitional regimes identified here, and seek to understand the role played by marginally active fines i) in the susceptibility of gap-graded assemblies to internal erosion and ii) in the triggering of mechanical instabilities. As an additional perspective, the distinct characteristics of the regimes shown in this study will prove useful in the development of micromechanical models for gap-graded materials in which the typical mesoscale grain arrangements can be tailored for each regime.

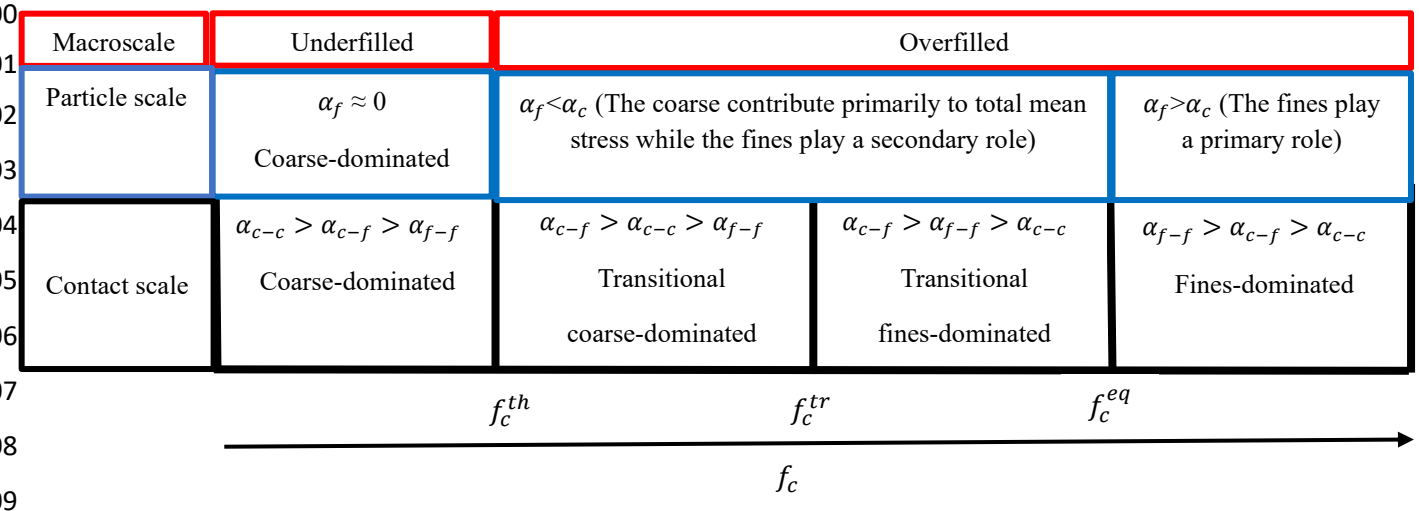

Fig. 21 Regime identification by macroscale, particle scale and contact scale characteristics

Notations

C	Total number of contacts in a granular system
C_{c-c}^{t}	The proportion of all contact types belonging to the c-c contacts
C_{c-f}^{t}	The proportion of all contact types belonging to the c-f contacts
C_{f-f}^{t}	The proportion of all contact types belonging to the f-f contacts
C_{wl}^{t}	The proportion of all contact types belonging to the wall
C_{n}^{f}	Proportion of the total number contacts belonging to the finer fraction
C_{n}^{c}	Proportion of the total number contacts belonging to the coarser fraction
d_{50}	Mean size of the fine grains
D_{50}	Mean size of the coarse grains
$e_{\max}$	Maximum void ratio
$e_{\min}$	Minimum void ratio
e_{crit}	Void ratio at the critical state
e_{hc}	Void ratio of the host sand
e_{hf}	Void ratio of the silt
ε_a	Axial strain (in *y*-direction)
ε_q	Deviatoric strain
$\varepsilon_{\mathrm{vol}}$	Volumetric strain
f_c	Fines content
f_{th}	Threshold fines content
f_c^{th}	Threshold fines content
f_c^L	Limiting fines content
f_j^c	Contact force vector
l	Unit branch vector
N_p	Number of particles in the granular system
N_c	Number of contacts in a granular system
N_p^c	Number of coarse particles in the system
N_p^f	Number of fine particles in the system
N_c^p	Number of contacts involving a particle
N_0	Number of particles with no contact
N_1	Number of particles with one contact
$N_{c\geq 1}$	Number of coarse particles with one or more contacts
$N_{f\geq 1}$	Number of fine particles with one or more contacts
NC_f	Normalised total contacts for the coarser fraction
NC_f	Normalised total contacts for the finer fraction
n_i	Unit branch vector
p	Mean effective stress
p^c	Mean stress transmitted by the coarser fraction
p^f	Mean stress transmitted by the finer fraction
p^k	Mean stress transmitted by a contact type
P^p	Particle mean stress
$\overline{P^p}$	Average particle mean stress
α_c	Proportion of the total mean stress transmitted by the coarser fraction
α_f	Proportion of the total mean stress transmitted by the finer fraction
α_k	Proportion of the total mean stress transmitted a contact type
$(q/p)_{max}$	Stress ratio at the peak
$(q/p)_{crit}$	Stress ratio at the critical state

q	Deviatoric stress
q^f	Deviatoric stress transmitted by the finer fraction
q^c	Deviatoric stress transmitted by the coarser fraction
q_f	Proportion of the deviatoric stress transmitted by the finer fraction
R-squared	Goodness of fit
R_d	Ratio of the mean size of the coarse grains to the mean size of the fine grains
R_p	Radius of particle
R_1	Radius of first particle in contact
R_2	Radius of second particle in contact
R_f	Proportion of non-active fines
e_{skel}	Skeleton void ratio
$e_{skel};x$	Skeleton void ratio determined using a threshold coefficient
Skl_f	Proportion of fines included in skeleton
x	Threshold coefficient
μ_{prep}	Inter-particle friction coefficient during assembly preparation (isotropic compression)
μ	Inter-particle friction coefficient
λ	Size fraction
V	Volume of system
V^p	Volume of particle
σ_{zz}	Normal stress in *z*-direction
σ_{yy}	Normal stress in *y*-direction
σ_{xx}	Normal stress in *x*-direction
σ_{ij}	Second order stress tensor
σ_{ij}^c	Second order stress tensor for all contacts
σ_{ij}^p	Second order stress tensor for a particle
σ_p^c	Average mean stress transmitted by the coarser fraction
σ_p^f	Average mean stress transmitted by the finer fraction
ϕ	Friction angle
ϕ_p	Peak friction angle
ϕ_c	Critical state friction angle
ψ_{max}	Maximum dilatancy angle
Z	Mean coordination number
Z_{ini}	Mean coordination number at the initial state (after isotropic compression)
Z_{crit}	Mean coordination number at the critical state
Z_g	Geometrical coordination number
Z_{gc}	Geometrical coordination number for coarse particles
Z_{gf}	Geometrical coordination number for fine particles
Z_m	Mechanical coordination number
Z_{mc}	Mechanical coordination number for coarse particles
Z_{mf}	Mechanical coordination number for fine particles

Appendix A. REV scale analysis

In order to confirm that the sample size of 100,000 particles used for all f_c in this study is a representative element volume (REV), in Fig. A.1, we show that increasing the assembly size to 200,000 particles for both the dense and loose assemblies having f_c = 30% did not significantly influence the stress-strain responses. The slight sensitivity to assembly size observed in the volumetric strains was also reported in the DEM study on REV for granular materials by Adesina et al., (2022) and can be attributed to the small variation in the initial void ratio of the assemblies. The REV test is shown here for f_c = 30% because it represents the threshold fines content and is the fines content with the highest coarse-fine particle interaction (Fig. 17) which indicates the largest REV size.

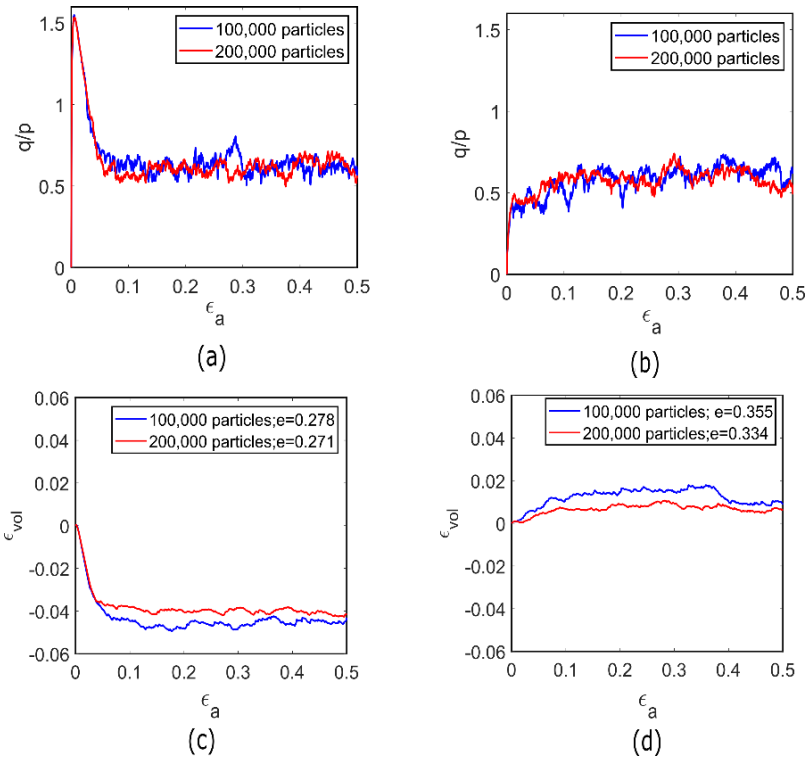

Fig. A.1 Effect of assembly size on (i) the stress-strain responses for dense assemblies (μ_{prep}=0.03) and (ii) loose assemblies (μ_{prep}=0.5) (iii) volumetric strain responses for the dense assemblies and (iv) the loose assemblies having f_c = 30%

Appendix B. Fine contribution to deviatoric stress

Fig. A.2 shows the evolution of the proportion of the deviatoric stress, q, transmitted by the fines during shearing, for dense and loose assemblies of different fines content, f_c. Provided that all stress tensors are diagonal in the frame (x, y, z), the deviatoric stress for the entire system is calculated as:

$$q = \sigma_{zz} - (\sigma_{xx} + \sigma_{yy})/2 \qquad (A1)$$

Similar to the mean stress (see Section 4), the proportion of the total deviatoric stress transmitted by the finer fraction, q_f, is calculated as q^f/q, while the proportion of the total deviatoric stress transmitted by the coarser fraction, q_f, is calculated as q^c/q, where q^f and q^c are the deviatoric stress transmitted by the finer and the coarser populations, respectively.

As expected, the q_f data is generally similar to the α_f data presented in Fig. 9. It is worthy of note that the q_f data presented in Fig. A2 starts after the initial state, at ϵ_a = 0.02, since $q = 0$ at the initial state. We observed that for $f_c \geq 30\%$, the magnitude of q_f is lower than the magnitude of α_f during shearing. This indicates that the stress is more isotropic in the finer fraction than in the coarser fraction.

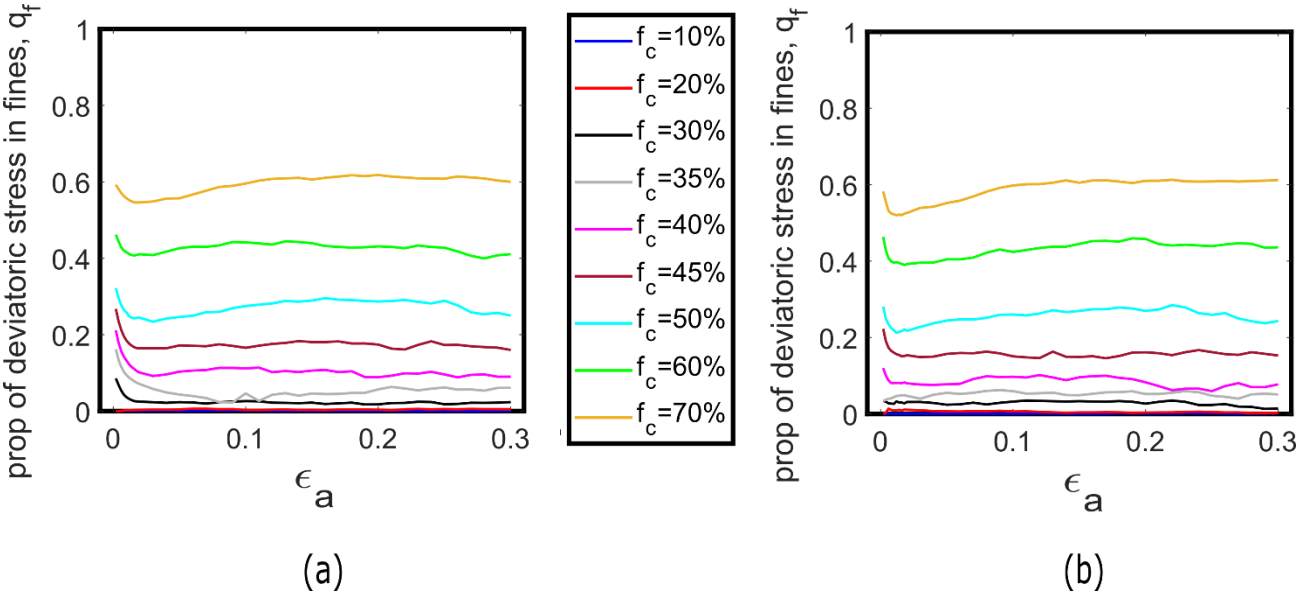

Fig. A.2 Evolution of the proportion of deviatoric stress transmitted by the fines during shearing for (a) dense assemblies (b) loose assemblies

Appendix C. Sensitivity analysis to the threshold coefficient used in the definition of the skeleton void ratio.

In Table A.1 and Fig. A.3, we show that at the critical state, $e_{skel}; x = 0.1$ exhibited a negative correlation with $(q/p)_{crit}$ and yielded the highest R-squared value (R^2=0.84), while both the e and e_{mech} do not correlate with $(q/p)_{crit}$. $e_{skel}; x = 0.05$ and $e_{skel}; x = 0.25$ also yielded a negative correlation with $(q/p)_{crit}$, with R^2=0.73 and R^2=0.76, respectively. $e_{skel}; x = 1$ yielded a poor corelation (R^2=0.08) with $(q/p)_{crit}$, indicating that using a threshold coefficient, $x = 1$, for the skeleton void ratio calculation for the gap-graded assemblies, resulted in the exclusion of important stress-transmitting fines, especially from the overfilled assemblies. $x = 1$ is the standard for defining force-chains for narrowly-graded assemblies (Peters et al., 2005). In agreement with earlier studies (Adesina et al., 2023; Holubec & D'Appolonia, 1973; Ng, 2004), at the peak, e, correlates negatively with $(q/p)_{max}$, and yielded the highest R-squared value (R^2=0.97), followed by e_{mech} (R^2=0.66). e_{skel} correlated poorly with $(q/p)_{max}$.

Table A.1 Assessment of void ratio indexes with the strength value, (q/p)

Void ratio index	e	e_{mech}	e_{skel}; x=0.05	e_{skel}; x=0.10	e_{skel}; x=0.25	e_{skel}; x=1.0
R^2_{peak}	0.965	0.656	0.119	0.074	-	9.55e-5
R^2_{crit}	-	0.208	0.725	0.844	0.764	0.08

Note: The R^2 values here are determined from inverse relationship between strength and void ratio. '-' means strength increased with void ratio as against established relationship between strength and void ratio.

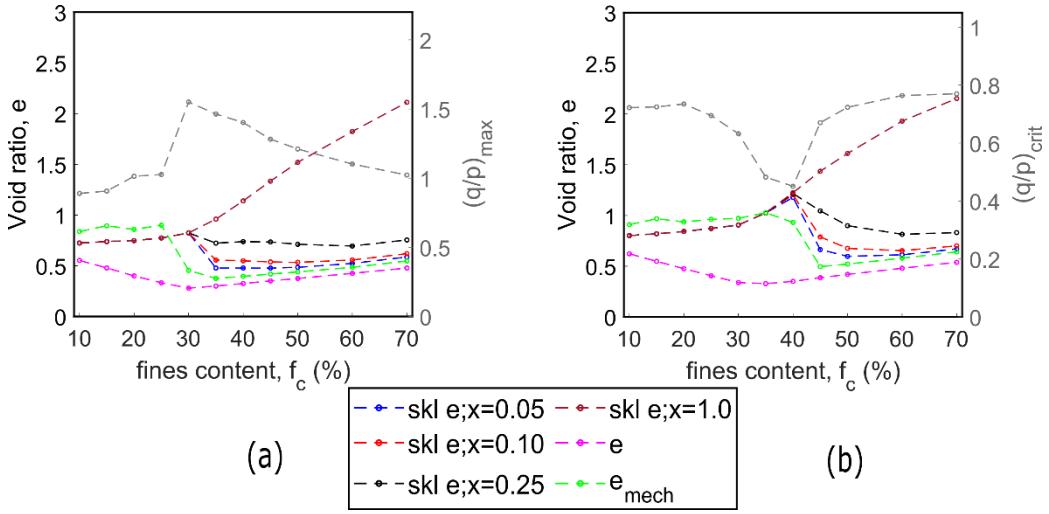

Fig. A.3 Relationship between (a) void ratio indexes and peak q/p, $(q/p)_{max}$ (b) void ratio indexes and critical state q/p, $(q/p)_{crit}$

Acknowledgement

This work was supported by the National Research Agency (ANR), France. It is a product of the research project titled "Micro-scale driven Models for Discrete for Discrete Materials (MiMoDiM)", with the reference, ANR-22-CE46-0001. A CC-BY public copyright license has been applied by the authors to the present document and will be applied to all subsequent versions up to the Author Accepted Manuscript arising from this submission, in accordance with the grant's open access conditions.

Credit Authorship

Peter Adesina: Conceptualization, Methodology, Investigation, Formal analysis, Visualization, Writing – original draft.

Antoine Wautier: Funding acquisition, Conceptualization, Methodology, Supervision, Writing – review & editing.

Nadia Benahmed: Conceptualization, Methodology, Supervision, Writing – review & editing.

Compliance with ethical standards

Conflict of interest The authors declare that there is no conflict of interests regarding the publication of this article. Publication has been approved by all authors. None of the material presented in the paper is submitted or published elsewhere.

References

Adesina, P. A., O'Sullivan, C., & Wang, T. (2023). DEM study on the effect of particle shape on the shear behaviour of granular materials. *Computational Particle Mechanics*, *Accepted*.

Adesina, P., O'Sullivan, C., Morimoto, T., & Otsubo, M. (2022). Determining a representative element volume for DEM simulations of samples with non-circular particles. *Particuology*, *68*, 29–43. https://doi.org/10.1016/j.partic.2021.10.007

Adesina, P., O'Sullivan, C., & Wang, T. (2024). Understanding the interplay between particle shape, grading and sample density on the behaviour of granular assemblies: A DEM approach. *Granular Matter*, *26*(1). https://doi.org/10.1007/s10035-023-01383-2

Bagi, K. (1999). Microstructural stress tensor of granular assemblies with volume forces. *Journal of Applied Mechanics, Transactions ASME*, *66*(4), 934–936. https://doi.org/10.1115/1.2791800

Benahmed, N., Nguyen, T. K., Hicher, P. Y., & Nicolas, M. (2015). An experimental investigation into the effects of low plastic fines content on the behaviour of sand/silt mixtures. *European Journal of Environmental and Civil Engineering*, *19*(1), 109–128. https://doi.org/10.1080/19648189.2014.939304

Bolton, M. D. (1986). The strength and dilatancy of sands. *Geotechnique*, *36*(1), 65–78.

Chang, C. S., & Yin, Z. Y. (2011). Micromechanical modeling for behavior of silty sand with

influence of fine content. *International Journal of Solids and Structures*, *48*(19), 2655–2667. https://doi.org/10.1016/j.ijsolstr.2011.05.014
Cubrinovski, M., & Ishihara, K. (2002). Maximum and minimum void ratio characteristics of sands. *Soils and Foundations*, *42*(6), 65–78. https://doi.org/10.3208/sandf.42.6_65
Cundall, P. A., & Strack, O. D. L. (1979). A discrete numerical model for granular assemblies. *Geotechnique*, *30*(3), 331–336. https://doi.org/10.1680/geot.1980.30.3.331
da Cruz, F., Emam, S., Prochnow, M., Roux, J., & Chevoir, F. (2005). Rheophysics of dense granular materials : Discrete simulation of plane shear flows. *PHYSICAL REVIEW*, *72*(February), 1–17. https://doi.org/10.1103/PhysRevE.72.021309
Deng, N., Wautier, A., Tordesillas, A., Thiery, Y., Yin, Z. Y., Hicher, P. Y., & Nicot, F. (2022). Lifespan dynamics of cluster conformations in stationary regimes in granular materials. *Physical Review E*, *105*(1), 1–15. https://doi.org/10.1103/PhysRevE.105.014902
Evans, D. M., & Zhou, S. (1995). Liquefaction Behaviour of Sand-Gravel Composites. *Journal of Geotechnical and Geoenvironmental Engineering*, *121*(3), 287–298.
Garner, S. J., & Fannin, R. J. (2010). Understanding internal erosion: a decade of research following a sinkhole event. *International Journal on Hydropower and Dams*, *17*(3), 93–98.
Holubec, I., & D'Appolonia, E. (1973). Effect of particle shape on the Engineering Properties of Granular Soils. *Evaluation of Relative Density and Its Role in Geotechnical Projects Involving Cohesionless Soils, ASTM STP 523*, 304–318. https://doi.org/10.1051/epjconf/201714006006
ICOLD. (2013). *Internal Erosion of Existing Dams, Levees and Dykes, and Their Foundations. In: Bridle, R. and Fell, R., Eds., Bulletin 164, Volume 1: Internal Erosion Processes and Engineering Assessment, International Commission on Large Dams, Paris.*
ICOLD, I. C. on L. dams. (2017). *ICOLD Bulletin 164 on Internal erosion of existing dams, leeves and dikes, and their foundations*.
Jiang, M. D., Yang, Z. X., Barreto, D., & Xie, Y. H. (2018). The influence of particle-size distribution on critical state behavior of spherical and non-spherical particle assemblies. *Granular Matter*, *20*(4), 1–15. https://doi.org/10.1007/s10035-018-0850-x
Kuerbis, R. H. (1989). Effect of gradation and fines content on the undrained response of sand. In *Department of Civil Engineering, The University of British Columbia*. https://doi.org/10.1016/0148-9062(90)90054-6
Lade, P. V., Liggio, C. D., & Yamamuro, J. A. (1998). Effects of Non-Plastic Fines on Minimum and Maximum Void Ratios of Sand. *Geotechnical Testing Journal*, *21*(4), 336–347. https://doi.org/10.1520/gtj11373j
Lade, P. V., & Yamamuro, J. A. (1997). Effects of nonplastic fines on static liquefaction of sands. *Canadian Geotechnical Journal*, *34*(6), 918–928. https://doi.org/10.1139/t97-052
Li, W., Chu, Y., Deng, G., Cai, H., Xie, D., & Lee Lee, M. (2023). Study of shear induced stress redistribution in gap-graded soils by discrete element method. *Computers and Geotechnics*, *156*(June 2022), 105248. https://doi.org/10.1016/j.compgeo.2023.105248
Li, Y., Otsubo, M., Ghaemi, A., Dutta, T. T., & Kuwano, R. (2022). Transition of gap-graded soil fabric – shear wave measurements and dispersion relation. *Soils and Foundations*, *62*(1), 101092. https://doi.org/10.1016/j.sandf.2021.101092
Liu, D., Morimoto, T., Carraro, J. A. H., & O'Sullivan, C. (2022). A semi-empirical re-evaluation of the influence of state on elastic stiffness in granular materials. *Granular Matter*, *24*(2). https://doi.org/10.1007/s10035-022-01215-9
Minh, N. H., Cheng, Y. P., & Thornton, C. (2014). Strong force networks in granular mixtures. *Granular Matter*, *16*(1), 69–78. https://doi.org/10.1007/s10035-013-0455-3

Ng, T.-T. (2004). Triaxial Test Simulations with Discrete Element Method and Hydrostatic Boundaries. *Journal of Engineering Mechanics*, *130*(10), 1188–1194. https://doi.org/10.1061/(asce)0733-9399(2004)130:10(1188)

Ni, Q., Tan, T. S., Dasari, G. R., & Hight, D. W. (2004). Contribution of fines to the compressive strength of mixed soils. *Geotechnique*, *54*(9), 561–569. https://doi.org/10.1680/geot.2004.54.9.561

Nicot, F., Hadda, N., Guessasma, M., Fortin, J., & Millet, O. (2013). On the definition of the stress tensor in granular media. *International Journal of Solids and Structures*, *50*(14–15), 2508–2517. https://doi.org/10.1016/j.ijsolstr.2013.04.001

Otsubo, M. (2016). *Particle Scale Analysis of Soil Stiffness and Elatic Wave Propagation*.

Peters, J. F., Muthuswamy, M., Wibowo, J., & Tordesillas, A. (2005). Characterization of force chains in granular material. *Physical Review E - Statistical, Nonlinear, and Soft Matter Physics*, *72*(4), 1–8. https://doi.org/10.1103/PhysRevE.72.041307

Pitman, T. D., Robertson, P. K., & Sego, D. C. (1994). Influence of fines on the collapse of loose sands. *Canadian Geotechnical Journal*, *31*(5), 728–739. https://doi.org/10.1139/t94-084

Rahman, M. M., Lo, S. R., & Gnanendran, C. T. (2008). On equivalent granular void ratio and steady state behaviour of loose sand with fines. *Canadian Geotechnical Journal*, *45*(10), 1439–1456. https://doi.org/10.1139/T08-064

Salgado, R., Bandini, P., & Karim, A. (2000). Shear Strength and Stifness of Silty Sand. *Journal of Geotechnical and Geoenvironmental Engineering*, *126*(5), 451–462.

Sarkar, D., Goudarzy, M., König, D., & Wichtmann, T. (2020). Influence of particle shape and size on the threshold fines content and the limit index void ratios of sands containing non-plastic fines. *Soils and Foundations*, *60*(3), 621–633. https://doi.org/10.1016/j.sandf.2020.02.006

Shire, T. (2014). *Micro-scale Modelling of Granular Filters. Thesis submitted to the Department of Civil and Engineering Civil and Environmental Engineering, Imperial College, London, United Kingdom.*

Shire, T., O'Sullivan, C., & Hanley, K. J. (2016). The influence of fines content and size-ratio on the micro-scale properties of dense bimodal materials. *Granular Matter*, *18*(3). https://doi.org/10.1007/s10035-016-0654-9

Shire, T., O'Sullivan, C., Hanley, K. J., & Fannin, R. J. (2014). Fabric and Effective Stress Distribution in Internally Unstable Soils. *Journal of Geotechnical and Geoenvironmental Engineering*, *140*(12), 04014072. https://doi.org/10.1061/(ASCE)GT.1943-5606.0001184

Skempton, A., & Brogan, J. (1994). Experiments on piping in sandygravels. *Géotechnique*, *44*(3), 449–460.

Skempton, A. W., & Brogan, J. M. (1994). Experiments on piping in sandy gravels. *Geotechnique*, *44*(3), 449–460. https://doi.org/10.1680/geot.1995.45.3.565

Šmilauer et al, V. (2021). *Yade Documentation 3rd ed. The Yade Project* (p. DOI:10.5281/zenodo.5705394 (http://yade-dem.org/do).

Sufian, A., Artigaut, M., Shire, T., & O'Sullivan, C. (2021). Influence of Fabric on Stress Distribution in Gap-Graded Soil. *Journal of Geotechnical and Geoenvironmental Engineering*, *147*(5), 1–14. https://doi.org/10.1061/(asce)gt.1943-5606.0002487

Thevanayagam, S. (1998). Effect of Fines and Confining Stress on Undrained Shear Strength of Silty Sands. *Journal of Geotechnical and Geoenvironmental Engineering*, *124*(6), 479–491. https://doi.org/10.1061/(asce)1090-0241(1999)125:11(1024)

Thevanayagam, S., & Mohan, S. (2000). Intergranular state variables and stress-strain behaviour of silty sands. *Geotechnique*, *50*(1), 1–23. https://doi.org/10.1680/geot.2000.50.1.1

Thevanayagam, S., Shenthan, T., Mohan, S., & Liang, J. (2002). Undrained Fragility of Clean Sands, Silty Sands, and Sandy Silts. *Journal of Geotechnical and Geoenvironmental Engineering*, *128*(10), 849–859. https://doi.org/10.1061/(asce)1090-0241(2002)128:10(849)

Thornton, C. (2000). Numerical simulations of deviatoric shear deformation of granular media. *Geotechnique*, *50*(1), 43–53. https://doi.org/10.1680/geot.2000.50.1.43

Thornton, C., & Anthony, S. J. (1998). Quasi-static deformation of particulate media. *Phil. Trans. R. Soc. Lond. A*, *356*, 2763–2782.

Thornton, Colin. (2015). Granular Dynamics, Contact Mechanics and Particle System Simulations: A DEM study. *Granular Dynamics, Contact Mechanics and Particle System Simulations: A DEM Study*, *24*, 1–195. https://doi.org/10.1007/978-3-319-18711-2

Tordesillas, A., Walker, D. M., & Lin, Q. (2010). Force cycles and force chains. *Physical Review E - Statistical, Nonlinear, and Soft Matter Physics*, *81*(1), 5–7. https://doi.org/10.1103/PhysRevE.81.011302

Vaid, Y. P. (1994). Liquefaction of silty soils. *In: Proceedings of Ground Failures Under Seismic Conditions. Geotech. Spec. Publ. 44, ASCE, New York*, 1–16.

Vaid, Y. P., & Sasitharan, S. (1992). The strength and dilatancy of sand. *Canadian Geotechnical Journal*, *29*, 522–526. https://doi.org/10.1680/geot.1987.37.4.517

Vallejo, L. E. (2001). Interpretation of the limits in shear strength in binary granular mixtures. *Canadian Geotechnical Journal*, *38*(5), 1097–1104. https://doi.org/10.1139/cgj-38-5-1097

Wang, T., Liu, S., Wautier, A., & Nicot, F. (2022). Updated skeleton void ratio for gravelly sand mixtures considering the effect of grain size distribution. *Canadian Geotechnical Journal*, *59*(11), 12–23. https://doi.org/10.1139/cgj-2021-0443

Wautier, A., Bonelli, S., & Nicot, F. (2018). Micro-inertia origin of instabilities in granular materials. *International Journal for Numerical and Analytical Methods in Geomechanics*, *42*(9), 1037–1056. https://doi.org/10.1002/nag.2777

Xiao, Y., Xiang, J., Liu, H., & Ma, Q. (2017). Strength–dilatancy relation of sand containing non-plastic fines. *Geotechnique Letters*, *7*(2), 204–210. https://doi.org/10.1680/jgele.16.00144

Yang, S., Lacasse, S., & Sandven, R. (2005). Determination of the Transitional Fines Content of Mixtures of Sand and Non-plastic Fines. *Geotechnical Testing Journal*, *29*(2), 102–107. https://doi.org/10.1520/GTJ14010

Yin, Z. Y., Zhao, J., & Hicher, P. Y. (2014). A micromechanics-based model for sand-silt mixtures. *International Journal of Solids and Structures*, *51*(6), 1350–1363. https://doi.org/10.1016/j.ijsolstr.2013.12.027

Zhu, H., Nguyen, H. N. G., Nicot, F., & Darve, F. (2016). On a common critical state in localized and diffuse failure modes. *Journal of the Mechanics and Physics of Solids*, *95*, 112–131. https://doi.org/10.1016/j.jmps.2016.05.026

Zhu, H., Nicot, F., & Darve, F. (2016). Meso-structure organization in two-dimensional granular materials along biaxial loading path. *International Journal of Solids and Structures*, *96*, 25–37. https://doi.org/10.1016/j.ijsolstr.2016.06.025

Zuo, L., & Baudet, B. A. (2015). Determination of the transitional fines content of sand-non plastic fines mixtures. *Soils and Foundations*, *55*(1), 213–219. https://doi.org/10.1016/j.sandf.2014.12.017